Projecte de Fi de Carrera

Enginyer Industrial

Biomechanics in batoid fishes

MEMÒRIA

Autor: Albert Comas Ollé
Director: Lorenzo Valdevit

Convocatòria: Octubre 2013

Escola Tècnica Superior
d'Enginyeria Industrial de Barcelona

ABSTRACT

Batoid fishes (e.g., manta rays) are extremely efficient swimmers, combining extreme strength and incredible maneuverability. Replicating these unique properties in synthetic autonomous under-water vehicles would have tremendous implications. Several research groups have been exploring these concepts for the past decade, and a small number of prototypes have been demonstrated. Importantly though, these prototypes match the batoid external motion (in terms of range of motion and actuation force) but do not employ a similar internal mechanics.

The configuration of skeletons and muscle structures for a number of different batoid fishes have been recently unveiled, presenting a unique opportunity to analyze the internal mechanics of these complex structures, and ultimately use the acquired understanding to realize truly bio-mimetic underwater vehicles.

As a whole wing has hundreds of moving elements, a full finite elements simulation of the entire wing is not feasible. To address this problem, we implemented a numerical model which will represent a part of the entire wing, and we investigated the effects of geometric and materials parameters on its stiffness. The length of each radial and the offset between them are going to be the most relevant variables and hence, the ones tested.

Furthermore, to represent efficiently all the wing, we calculated its effective elastic properties using rigorous homogenization theory. These properties could then be used in shell FE models of the entire wing, and capture spatial variation in elastic constants in a numerically efficient way. Within the context of this work, the stiff and compliant direction will be found and that will give us an idea of the ability of the model to capture the experimentally observed deformation patterns.

We observe that our 2D homogenized wing model fails to capture the substantial twisting/bending coupling that is observed experimentally. We speculate that the lack of torsional degree of freedom at the joints is responsible for this discrepancy.

Once this deformation mechanism is built into a model, future investigations can use the homogenized stiffness approach to extract an effective continuum-based representation of

ETSEIB

the response of the wing in a continuum shell finite element model. This element can then be used for efficient modeling of entire wings; this will allow efficient modeling of spatially non-uniform wing morphologies in a Finite Elements setting. Once the elastic response of the wing is completely characterized, efforts will need to focus on actuation.

CONTENTS

ABSTRACT 2

CONTENTS 4

INTRODUCTION 6

1 BACKGROUND 7

1.1 Biological Features Of Batoid Fishes 7

1.2 Advantageous features of batoid fishes 8

1.3 Limitations of a biomimetic product 8

2 BATOID FISH MIMICKING ROBOT DEVICES 9

3 MUSCULOSKELETAL SYSTEM OF A BATOID FISH 12

3.1 Radials 13

3.2 Muscles 14

4 MORPHOLOGY OF THE WING 15

4.1 Radial's location effect: Spring model 16

4.1.1 Effect of Joint Position on Stiffness 16

4.1.2 Effect of Joint Position on Bending Direction 18

5 FINITE ELEMENT ANALYSIS OF A PART OF THE WING 19

5.1 Geometry 19

5.2 Materials 20

5.3 Mesh, elements, and steps 22

5.4 Boundary conditions 22

5.5 Preliminary results 22

ETSEIB

5.6 Stiffness parameters 24
5.7 Results 25
5.7.1 Stiffness parameter: angle, α 25
5.7.2 Stiffness parameter: radial's length, l 28
5.8 Conclusions from the FEM analyses 29
6 HOMOGENIZED MODEL 30
6.1 Methods 30
6.2 Results 31
6.3 Conclusions from the homogenized model 33
7 CONCLUSIONS AND FUTURE WORK 35
ACKNOWLEDGMENTS 37
REFERENCES 38
ANNEX A: ABAQUS SCREENSHOTS 42
ANNEX B: MATLAB CODE 45

INTRODUCTION

For millions of years organisms in this planet have experienced an evolutionary process of natural selection and adaptation. This process has allowed the different species to solve problems for their survival by trial and error. As species have evolved through incredibly long times (much longer than any engineering system), several natural systems are believed to be near optimal. Therefore, nature can provide inspiration for the solution of engineering problems. Synthetic systems that mimic natural organisms are called *biomimetic*.

Aquatic propulsion is one of the areas where animals display efficiencies that are vastly superior to those of any synthetic machines. For example, traditional propulsion techniques such as screw propellers cannot provide the sophisticated level of maneuverability necessary for the development of the next generation of Autonomous Underwater Vehicles (AUVs). Furthermore, engines based on conventional propulsion systems are expensive to repair and have an unacceptably low efficiency. To overcome these limitations, over the past decade, numerous programs have sought to conceptualize and Bioinspired Autonomous Underwater Vehicles (BAUVs).

For decades, aquatic mammals, e.g., dolphins, have been the primary source of inspiration; unfortunately, synthetic biomimetic robots performed much worse than expected [11]. More recently, teams of biologists and engineers have started looking to batoid fishes to provide inspiration for the next generation of BAUVs [22].

The proposed research effort aims at elucidating the bio-mechanical behavior of the locomotion system of batoid fish: understanding the mechanics and actuation mechanisms that give these animals incredible strength and agility will provide invaluable guidance to the development of synthetic bio-inspired underwater vehicles.

1 BACKGROUND

1.1 Biological Features Of Batoid Fishes

Batoidea is a superorder of fish that includes thirteen families of skates, rays, sawfish, and guitarfish. They are closely related to sharks, having a cartilaginous body in common [8]. However, their dorsoventrally flattered bodies clearly distinguish them from sharks.

Although all batoid fishes generate waves through their fins by contracting their musculature, they can be classified into two big groups, based on their method of propulsion through water [21]. Sawfishes and guitarfishes are *undulatory* swimmers, displaying axial-based locomotion, undulating their body and/or shark-like tail (BCF); conversely, skates and rays are *oscillatory* swimmers, and use their greatly enlarged median paired fins (MPF) to achieve a pectoral-fin based locomotion by contracting specially the dorsal (upper) muscles [27].

Looking at the second group, although rays can have a similar morphology, their swimming mode can be notably different, describing a continuum between undulation and oscillation. Undulatory motion was called “rajiform” by Breder (1926) and defined as having one or more waves present on the fin at a time (f>1) [Webb, 1994]. By contrast, oscillators were termed “mobuliform” by Webb (1994) [33] and their movement resembles a flying bird flapping their wings, with less than half a wave on the wing at any time (f<0.5). Rosemberger (2001) suggested that undulatory locomotion produces better maneuverability, allows moving backwards and is more efficient at low speeds. On the

Figure 1 *Left: Undulatory swimmer (Dasyatis Americana) with an average of 1.1 waves across the wing at any time [27]. Right: Oscillatory swimmer (Rhinoptera bonasus), with an average of 0.4 waves [27].*

other hand, oscillators can achieve greater speeds to cover long swimming distances. Remarkably, it has been documented that Dasyatidae can switch between undulatory and oscillatory swimming [26].

1.2 Advantageous features of batoid fishes

Several nature propulsion systems are proved to have better efficiency and performance than engineered designs [10]. Engineered systems are large, they lose a great amount of energy into the wake, and many aquatic animals may be wounded even unto death by screw propellers [12]. In contrast, not only oscillatory propulsive movements intrinsic of fishes and marine mammals don't have these weak points but also provide an inherent maneuvering capability. Consequently, the next generation of underwater vehicles should have bio-inspired constitution [22]. However, natural systems are usually much bigger than most of the marine animals and problems of scaling can arise. That is one reason why manta rays are particularly interesting: some species can weigh more than 1,300 kg and measure more than 7 m in width, reasonable proportions for an AUV.

1.3 Limitations of a biomimetic product

Nevertheless, biomimetics has some limitations due to the inherent differences between engineered and animals such as materials or structures. While engineered materials are made of stiff materials like metals, ceramics, and plastics; animal ones are much more compliant but have the particularity of being self-repairing [10]. That explains why there is a lot of work to be done in that field in order to have a truly biomimetic product.

Another added difficulty when mimicking any animal is the complex amount of muscles they have along all their body. When modeling it, engineers face a moving body with an unreasonably big number of degrees of freedom to be actuated with their respective control and energy supply.

2 BATOID FISH MIMICKING ROBOT DEVICES

Many research groups have been exploring how to build a batoid fish swimming based robot during the last decade and some prototypes have been demonstrated. Without the aim of being exhaustive, this is the evolution of the more relevant advances.

In 2001 the first experimental undulating-fin device was developed [30]. What these researchers found immensely interesting was the particularity of the batoids locomotion mode that allowed them to move forward and backward. By a mathematical analysis and a prototype they proved their ability to generate reversible thrust.

Although some other fish robots had been assembled, it can be attributed to a University of British Columbia research group in 2002 to be the first who built a biomimetic robot based on a batoid fish, in this case a Gymnura micrura [2]. The robo-ray, albeit not succeeding in every goal as good as their creators would have wanted, it set the basis for further work. The group considered it a profiting project because in spite of not being able to propel itself in water, the robo-ray could emulate both undulaltory and oscillatory locomotion strategies. The actuation was given by the use of Shape Memory Alloys (SMA).

The thrust production and the wake structure of an oscillating fin were investigated [6]. An exhaust aerodynamic study using an artificial fin revealed how batoid fish were propelled and hence what requirements the biomimetic robots need to fulfill for the purpose of maximizing the thrust.

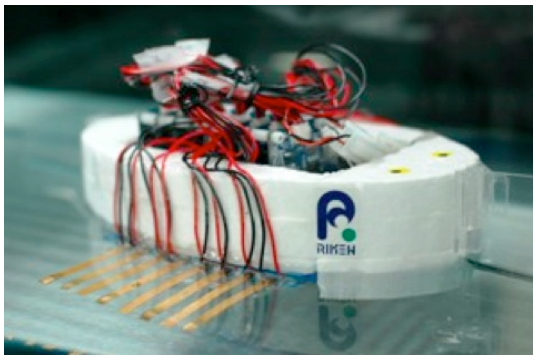

Figure 2 *Robot actuated with 8 IPMCs tomimic rajiform swimming [31].*

Some robots were manufactured trying diverse technologies to actuate the wing. Conductive polymers [32], electroactive polymers (EAP) [25], or ionic polymer-metal composite (IPMC) [31] played the role of the muscles. Other groups chose an external actuation of the wing with a rotational motor, planetary gear mechanism and spherical joint to effectuate all pectoral fin movements [18].

However, the aim of all progress exposed was to generate trust in an efficient way but maneuverability and stability are a key factor in an unmanned underwater vehicle which often operates near the seabed. Wing control becomes decisive and a research group compared a bang-bang with a PID control [14] using simulations and a prototype. It was proved that the PID was better.

On the one hand, Cownose Ray-I [34], which was inspired on the Rhinoptera bonasus, allowed the engineers to explore how the different parameters affect in the oscillatory motion (i.e. swimming while having less than half a wave at a time). They found the amplitude and the number of waves as the most determinant variables of the speed. They also tested how the asymmetric phase is more effective when swerving than increasing one side's amplitude. Some years later and based on Cownose Ray-I, the BHRay-I and BHRay-II [13]; and the Robo Ray II [35][3], and Robo Ray III [23] were presented being the reference of the mobuliform swimming robots.

On the other hand, NKF-II was built to explore the gymnotifrom swimming style, which is different from batoid fishes' locomotion mode. Nevertheless, NKF-II's wing was used to

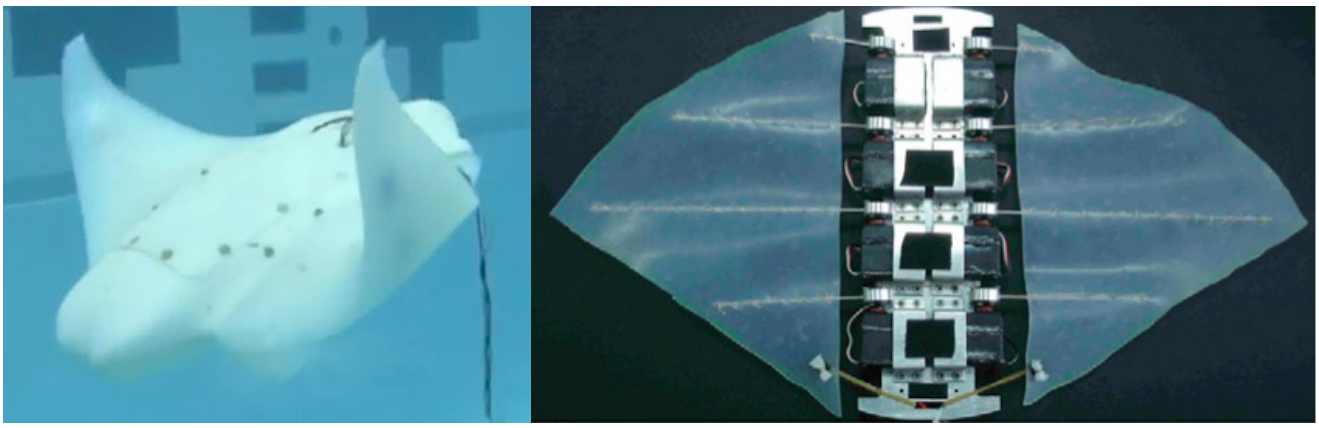

Figure 3 *Mantabot on the left [36] and Cownose Ray-I on the right [34].*

produce rajiform swimming. By connecting sliders they were able to reproduce different sinusoidal waveforms [19].

In 2010, in Japan was designed a prototype characterized for its simplicity [1]. Hence, it was robust and inexpensive to manufacture. A soft body that only had one insert in each wing configured the essential components of the robot. A servomotor oscillated the insert generating a wave, which was propagated along the body.

Advanced techniques were performed last year [35] and the latest robot release by a team lead by Hillary Bart-Smith form the University of Virginia was the Mantabot [36]. It uses tensegrity structures to propel himself with an oscillating swimming style. Although the power supply needs to be improved, probably it is the one that looks more like an actual animal and has more advanced swimming characteristics.

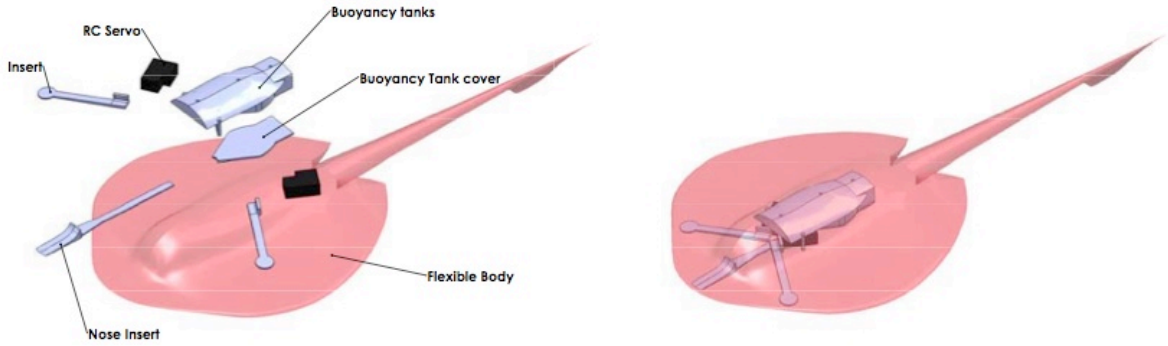

Figure 4 *Exploded view and assembly of a simple robot design mimicking a stingray [1] .*

Most of them consist of actuators arranged in a series and interconnected via a flexible material which allows them to mimic the movement. However, a lot of work needs to be done to build a truly BAUV capable of doing the exploration, rescue and all kind of missions that current AUV conduct.

It is believed that by mimicking not only the locomotion, but also imitating the internal mechanics of batoid fishes; a turning point on the development of next generation of underwater vehicles will be reached. Biologists and engineers need to work together and the current paper wants to make step forward into this fruitful cooperation.

3 MUSCULOSKELETAL SYSTEM OF A BATOID FISH

Batoid fishes have a dorsoventrally compressed body ranging in shape from circular to rhomboidal [7]. The pectoral skeleton is divided into two main parts: the fin rays and the pectoral girdle from where they emanate.

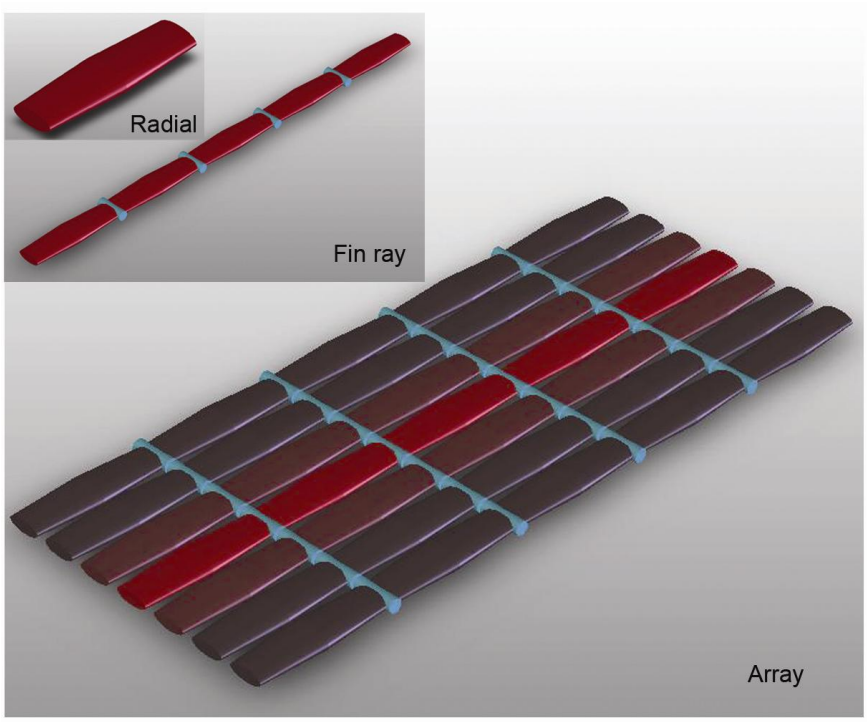

Figure 5 *The hierarchical structure of the batoid wing skeleton is composed of radials that are serially arranged into fin rays, which form a two dimensional array. Joint motion is constrained to act in a hinge-like fashion [29].*

The fin rays are long chains laterally oriented and they are constituted of serially-arranged small cylindrical cartilaginous elements, which are called radials. The distribution of the radials, its size, and shape determine de location of the joints between them, and hence, the biomechanical behavior of the wing [29]. Recent research has revealed that a cartilaginous skeleton is not as disadvantageous as previously thought compared to the ones made of bones [24].

3.1 **Radials**

The stiffness of each part of the wing is a crucial point to figure out the whole wing motion. The waves are propagated over an array composed by the radials which suffer a deflections and the joint which can be considered a mix of connective tissue and cartilage. Therefore, when the wing moves the joints act as hinges and the radials experience deflection.

$$Y_{max} = \frac{FL^3}{3EI} \qquad (1)$$

Where F is the muscle force, L is the length of the radial, E is the material stiffness and I is the second moment of area. Hence, the geometry (L and I) and the composition (E and I) will determine the stiffness of the radial.

The degree of mineralization of the radial is the primary variable responsible for its mechanical properties, given that mineralized cartilages is far more stiffer and stronger than unmineralized one. In the skeleton of batoid fishes, there are two different basic classes of calcification: crustal and catenated. The classification is based on whether the unmineralized core is completely covered by a thin layer of small tesserae, or just alongsome chains, respectively [5]. It was found that the degree of mineralization

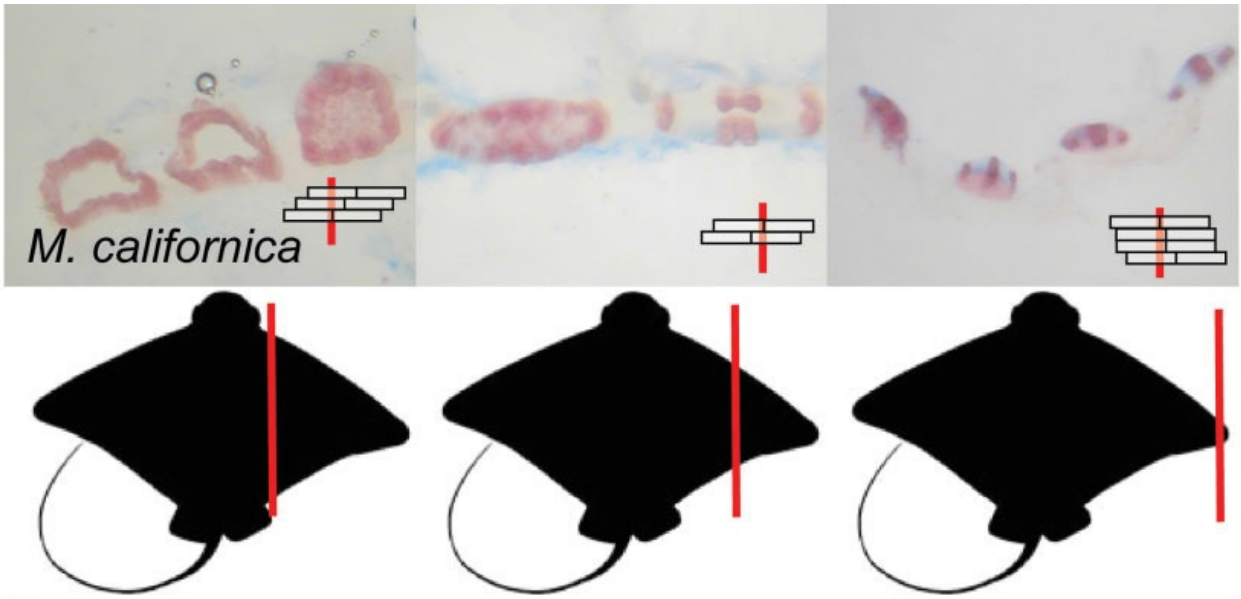

Figure 6 *Cross-section of calcification in Myliobatis californica skeletal elements from proximal, mid, and distal portions of the wing. Silhouettes show approximate area of wing from which sections were taken. Location of section in relation to joints is given by schematic in lower right corner of each panel [28].*

decreases with the increasing distance of the body axis until the distal end of a fin ray, i.e. crustal calcification is found in the proximal areas and catenated calcification near the edge of the wing. In the terminal radial, there is often only a single chain in its middle or a scattering of tesserae over its surface. The cross-sectional shape also becomes more dorsoventrally compressed distally [28].

The areolar calcification, that is nearly completely mineralized, only can be found in the vertebral column, from where fin rays emanate.

3.2 **Muscles**

Muscles are responsible for the actuation of the wing and, therefore, the locomotion of the fish. They emanate from the pectoral girdle and expand laterally over the fin rays with every single radial [16]. To make things more complex, there are some muscles that do not follow that fashion and are oriented perpendicular to fin ray to allow a better control. The most powerful stroke is provided by the dorsal abductor muscles, which are considerably more massive than the ventral abductors.

At this time, many details about the working of the muscular system are still largely unknown.

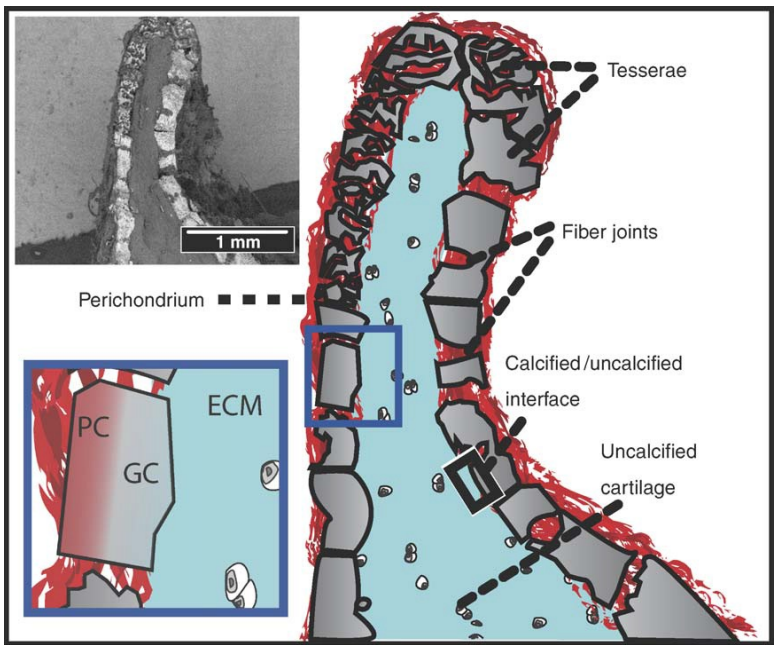

Figure 7 *Uncalcified and calcified phases of tessellated elasmobranch cartilage, depicted as a schematic of a cross-sectional backscatter electron micrograph of the lower jaw of the round stingray, Urobatis halleri (upper inset; white regions are calcified tissue). The lower inset provides an expanded view of the region bounded by the blue box, showing the arrangement of prismatic (PC) and globular (GC) calcification relative to the uncalcified cartilage matrix (ECM) and fibrous perichondrium [9].*

4 MORPHOLOGY OF THE WING

The disposition of the radials, and therefore the interradial joints, is so relevant on the locomotion of the animal that the pattern varies depending of the swimming style. In both cases, the range of motion between two adjacent radials in a fin ray is small (~15°) [28], but there are enough radials to allow great amplitude of movement to the edge of the wing.

Undulators, which have many waves moving along the wing, have smaller radials that decrease in size isometrically with the distance from the body axis and this results in the joints forming concentric lines [28]. On the other hand, oscillators, which appear to fly when swimming, have longer radials in the central areas of the wing. Additionally, a structure defined "cross-braces" was found in some species of oscillatory swimmers. These are connected radials that doesn't belong to the same fin ray but pertain to adjacent fin rays [28]. For both swimmers, each fin ray bifurcates and radials become shorter and smaller at some point close to the edge, and since this point is consistent for each fin ray, it forms a division line. Moreover, near the leading edge of some oscillators, some radials

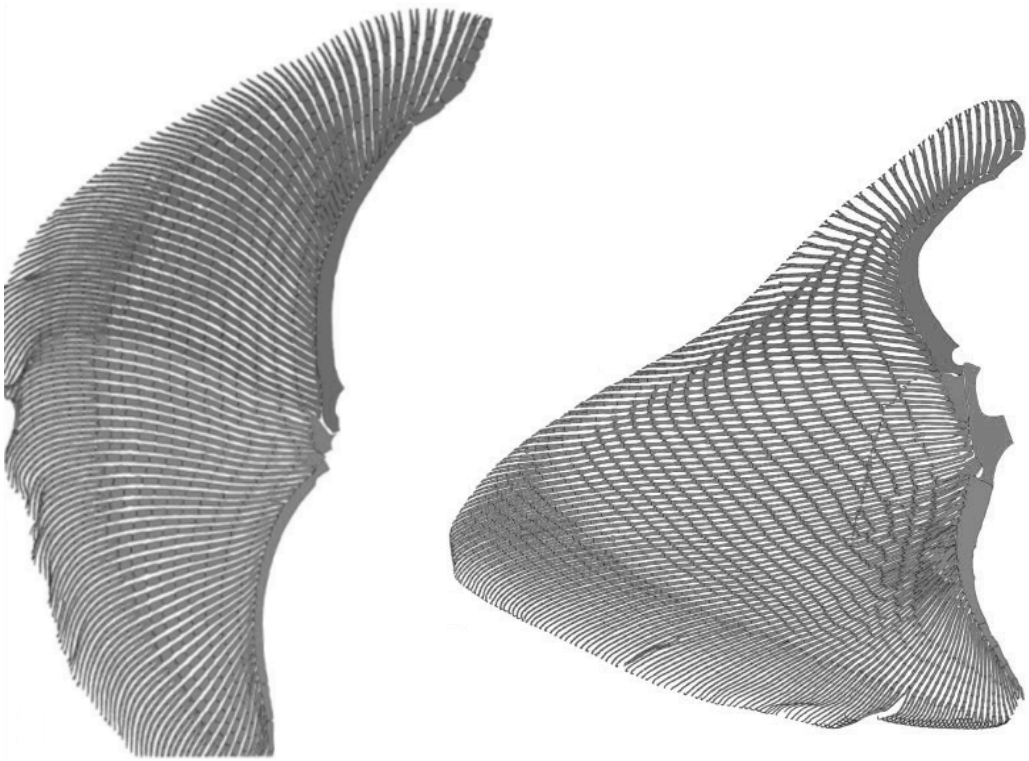

Figure 8 *Schematic outline and joint position of the wing skeleton of an undulator (Urobatis halleri) on the left and an oscillator (Gymnura crebripunctata) on the right [28].*

are laterally expanded so they fit closely together and form a nearly solid plate [28]. It can be also appreciated in *Figure 8* that the global shape of the wing also varies.

All these differences are attributed to the fact that, depending on the swimming strategy, different stiffened areas are needed. Oscillatory swimming requires large amplitude deformations of the wing so the bending is concentrated proximally. Conversely, travelling waves in undulators have shorter wavelength and decreased amplitude, thus concentrating bending stresses near the edges. More stiffness is expected in these bending areas [28].

Small changes on the morphology of the wing have serious repercussions on its mechanical properties. That is why analyzing and understanding its structure-properties relation is critical.

4.1 Radial's location effect: Spring model

J. Schaefer *et al.* studied how the configuration of the radials and joints affect the local stiffness and the bending properties of the wing; they adopted a linear spring model. Patterning of joint arrangement was believed to be an alternative mechanism of stiffening the wing to changing the radial's morphology [29]. Through high resolution radiographs of several species of batoids, the exact location of the joints was mapped. Key differences in joint's location were evident depending on the swimming style, i.e. oscillators vs undulators.

4.1.1 Effect of Joint Position on Stiffness

Modeling the connective tissue between radials as springs, Schaefer *et al.* used the energy as a proxy for stiffness. In an array, the mechanical behavior of a joint or a radial cannot be modeled without its neighbors because when a radial is moved, the connective tissue forces the neighbors to move as well. However, this effect decreases with distance and it was suggested that two radials per side where sufficient to extract information on wing stiffness. However, when calculating the energy of a 5-radial group, both sides are considered separately for simplicity and then they are added up to get the final result.

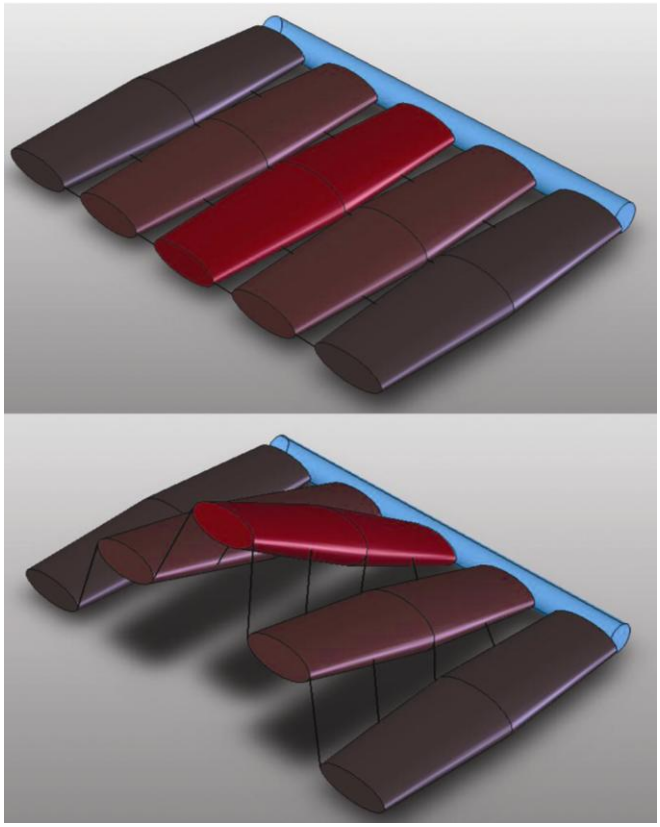

Figure 9 *Five radial system used to calculate localized stiffness. The top diagram is the basal configuration. The bottom diagram shows the system following perturbation of the central (primary) radial. The lateral-most (tertiary) radials on each side were constrained to remain unelevated. Lines joining radials symbolize elastic connective tissue [29].*

Given that radials are far stiffer than the connective tissue, i.e. joints, when a batoids wing is flexed, the bending occurs fundamentally at the joints. Thereby, in the model the radials are considered rigid bodies and the joints are represented by hinges. It is also assumed that the radials are attached to their neighbors along their entire length. By moving one joint closer or further away from the axis of bending of its neighbor joint, it can be bend "against" the neighboring radial instead of the joint, and is thus effectively stiffened [29].

Schaefer *et al.* found that the stiffness of a three-radial cell did not depend on the height of the tertiary radial (H_2, *Figure 10*) as much as on the height of the secondary radial (H_1). In his model, the maximum stiffness takes places when the secondary radial has negative height and the tertiary radial has a positive height, both compared to the primary radial [29]. Furthermore, the effect of the tertiary radial when the secondary radial has a positive height is negligible. This is represented in *Figure 10* on the right side of the plot, where the variation of stiffness only increases by making H_1 higher..

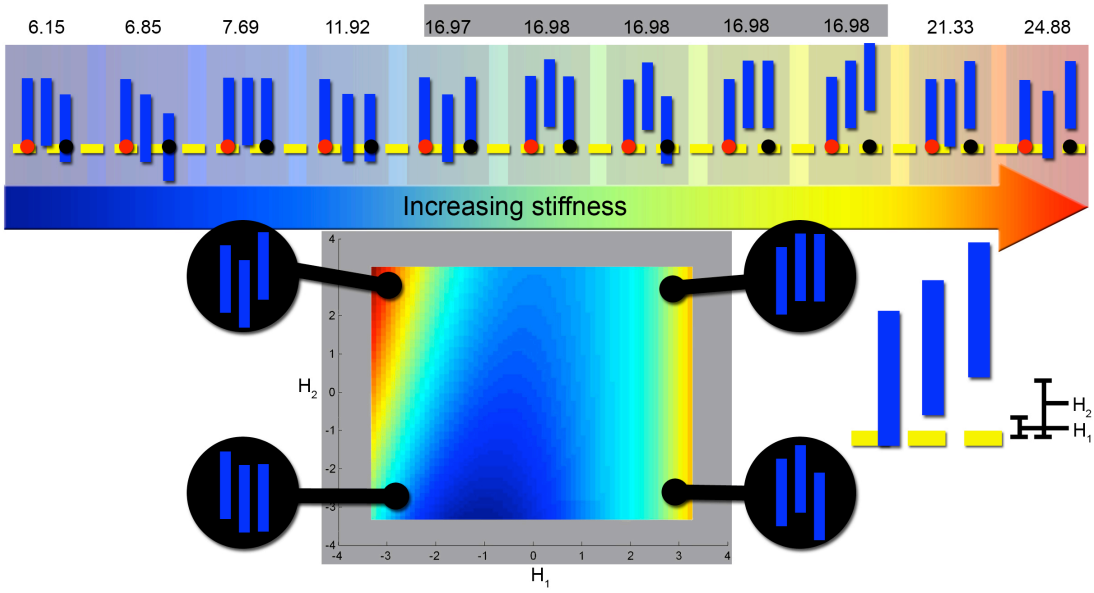

Figure 10 *Bending energies required for variations in H. Discrete arrangements of joints with varying values of H_1 and H_2 (groups of blue bars) are shown at the top. Degree of perturbation was kept constant. Red dots represent primary radials (perturbed). Black dots represent tertiary radials (constrained). Continuous variation of H_1 and H_2 results in the lower plot. There are several configurations that result in the same energy (highlighted) [29].*

Comparing oscillators and undulators, they were stiff medially and laterally, respectively. Major stiffness is needed in the areas were muscle force actuates because that prevents the wing from folding upon itself when acting against the water. The wing would curl with a radius of curvature too small when pulled by muscles if it was too flexible. Conversely, if it was too stiff it would buckle and it would be exceedingly energetically costly to bend [29].

4.1.2 Effect of Joint Position on Bending Direction

The bending direction was calculated as the normal line to the line formed by the offset of neighboring joints from the middle joint's plane of rotation [29]. Then these vectors were averaged, resulting in one direction for every five-radial group. Averaging all them, the result was a vector based on the geometry of the whole wing. Defining the 0° as the normal to the longitudinal axis of the animal and oriented to the animal, undulators showed a minimal offset and oscillators had a divergence around 20° pointing toward the front of the animal.

5 FINITE ELEMENT ANALYSIS OF A PART OF THE WING

Given that the literature cited so far confirms that the batoid's pectoral wing is a unique source of inspiration for next generation of AUVs, in this work we suggest a new modeling approach based on Finite Elements Analysis. The commercial software ABAQUS was used for all simulations. As a whole wing has hundreds of moving elements and a full finite element simulation of the entire wing is not feasible, the final objective of this work is the development of a methodology to extract the effective properties of the wing to model it as an anisotropic shell.

First of all, it is important to understand how some geometric parameters of the wing affect its local stiffness.

5.1 Geometry

The geometry used to model our problem is 2-dimensional shell with a rectangular shape (94mm by 144mm), encompassing more than 50 radials. This size was chosen as a compromise between computational efficiency and negligible edge effects.

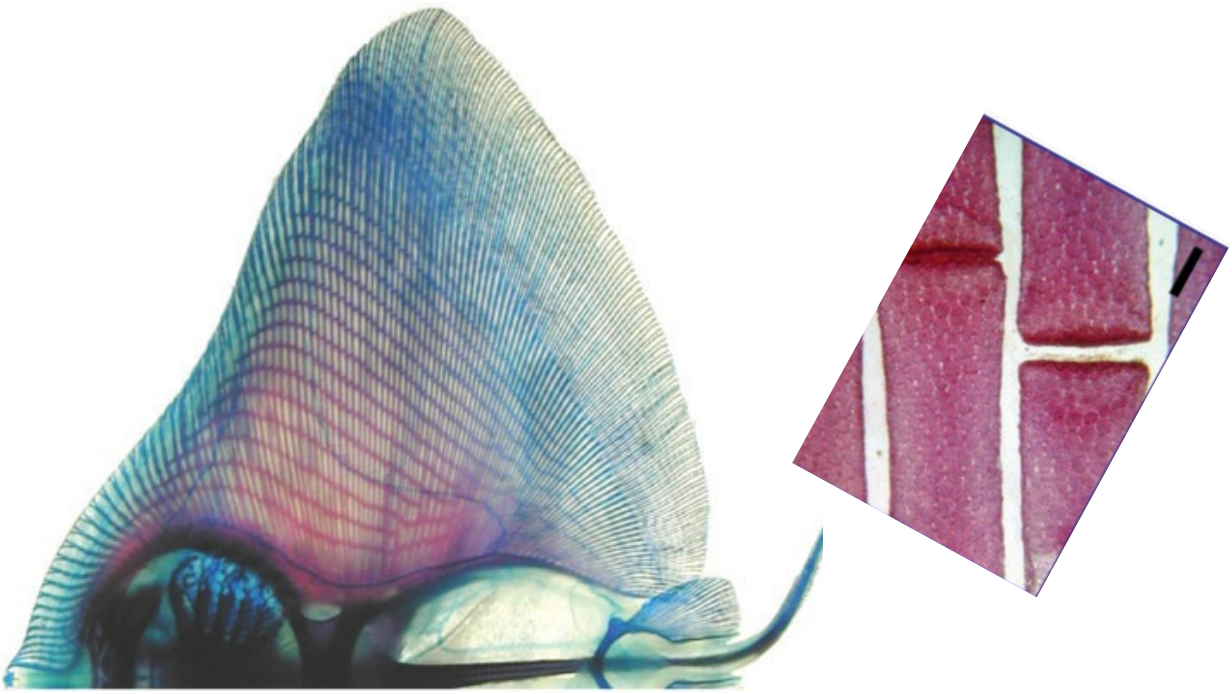

Figure 11 *Dorsal view of the wing and zoom showing the pattern. Calcified material (i.e. radials) is stained red [28].*

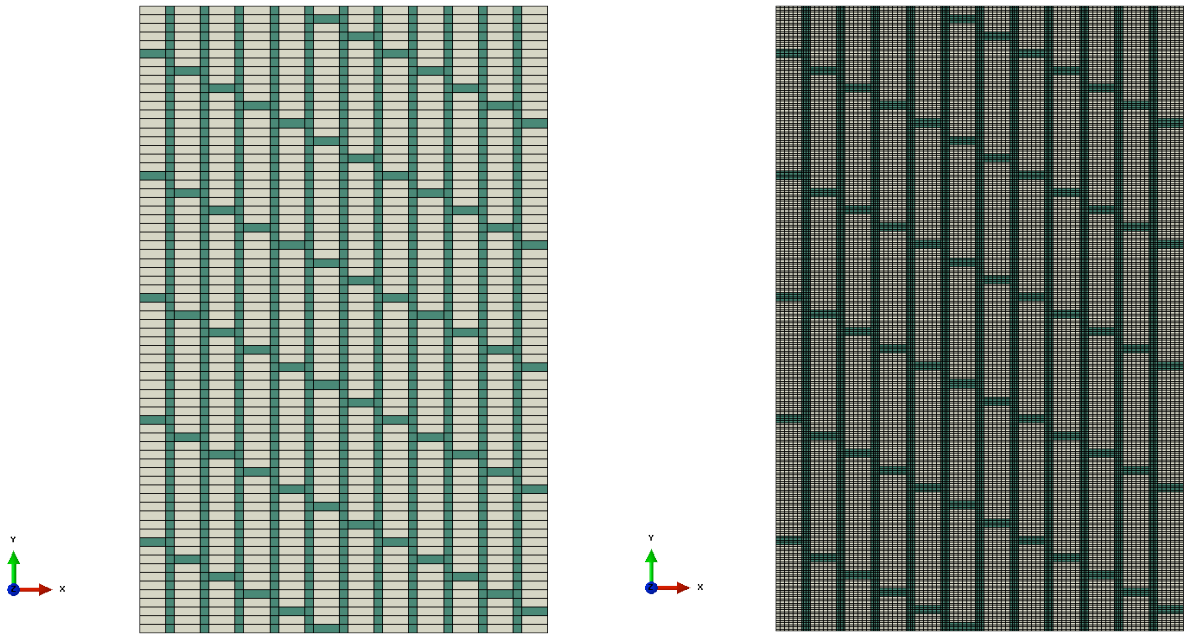

Figure 12 *Geometry of the model being yellow the radials, and green the joints. Each small rectangle is considered a single unit. On the right the model is meshed.*

The location of the radials and joint were decided based on existing high resolution radiographs [29]. Although some parameters will be changed to see how they effect on the properties of the wing, the model shown in *Figure 12* can be considered a representative model. It consists of 12 fin rays, with radials aligned with an offset of 26.57°. Each joint layer has 2 mm of width and each radial has a dimension of 26 mm by 6 mm. In all our models the thickness will be kept constant and equal to 6 mm. Hence, the radials have a square cross-section of 36 mm2. Although the dimensions of the radials and the joints vary depending on the location in the wing, our present model is periodic and ignores those variations.

5.2 **Materials**

Modeling the material properties can be a challenging task, due the difficulty in finding material models capable of representing the particularities of living materials.

Batoid fishes have a cartilaginous skeleton, but we can distinguish between two different materials: the radials, which have an uncalcified core covered by tesserae and play the structural role of a bone, and the mixture of connective tissue and unclacified cartilage surrounding the radials, which is termed “joint”.

Radials are modeled as an isotopic material with a linear elastic behavior. Hence, the Young's modulus, E, and the Poisson's ratio, ν, are enough to characterize it for a static analysis. From the biology, mechanics, and material science literature [17][20], values of E_{radial}=2600 MPa and ν_{radial}=0.5 were chosen.

Joints are uncalcified cartilage and as such have an intrinsic viscoelastic behavior. Not many experiments have been found on the literature on this material, so we consider valid the hypothesis of Porter et al. [24] who said that the composition of elasmobranchs and mammalian cartilage has similar composition. That is why we decided to take cartilage material properties from human knee joint cartilage, a far better studied problem.

Many materials models have been used but, of course, the election between one and the other will be based on what is the purpose of the research. Models such as biphasic or viscoelastic, among others, may be needed [29]. However, considering that when a batoids

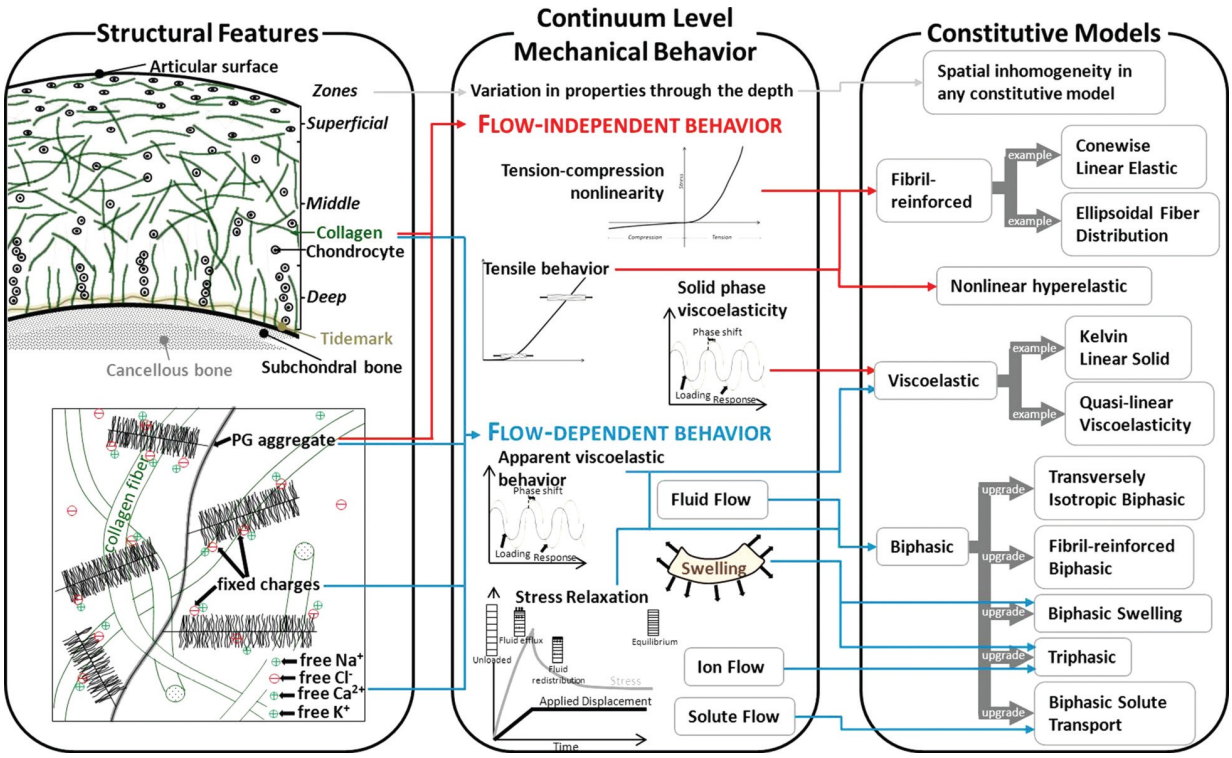

Figure 13 *Cartilage structural features, continuum level mechanical behavior, and constitutive models. Left panel—The structure and orientation of collagen and proteoglycan aggregates drive continuum mechanical behavior. Middle panel—Key features of continuum mechanical behavior include tension-compression nonlinearity, anisotropy, viscoelastic material behavior, and swelling. Right panel—Constitutive models capture certain features of cartilage behavior. As a general rule, the simplest constitutive model that captures the behavior of interest should be chosen [15].*

swims it involves frequencies greater than 1 Hz and we want to study the macromechanics of that system, the linear elastic model is accurate enough for our analysis.

Again, a single value for the Young's modulus and Poisson's ratio of the joint material does not exist, as it varies significantly from one species to the other. Furthermore, it has been difficult to perform accurate stiffness measurements, due to the small dimension and the time-dependence of the material. However, given that joint's stiffness is two orders of magnitude lower than radial's one, the exact value for a qualitative analysis is not that important. E_{joint}=25 MPa and ν_{joint}=0.5 were used in all simulations.

5.3 Mesh, elements, and steps

We used a 2D shell to represent our wing considering that the thickness (6 mm) is much smaller than the width (94 mm) and depth (144 mm). The mesh used is a 4-node shell element with linear interpolation. The mesh refined on the joints where strain is larger having each joint element half the area of a radial element.

Since there are going to be large deformations, nonlinear geometry must be allowed.

5.4 Boundary conditions

In all our simulations, the bottom edge is constrained, i.e., no displacement (U_x=U_y=U_z=0) and no rotation (UR_x=UR_y=UR_z=0). Fin rays emanate from the pectoral girdle, which is more calcified than the radials, and thus stiffer. Hence, it seems realistic that while the top edge bends, the bottom edge remains fixed.

On the opposite edge, we are going to apply a force always normal to the plane of the shell. Either a single node or the entire edge will be loaded, depending on the focus of each simulation.

5.5 Preliminary results

First of all we want to see how the different 3-radials configurations make the stiffness of the wing change. We applied force on the top edge and extracted the z-displacement, i.e., the out-of-plane displacement, of the top right and top left nodes.

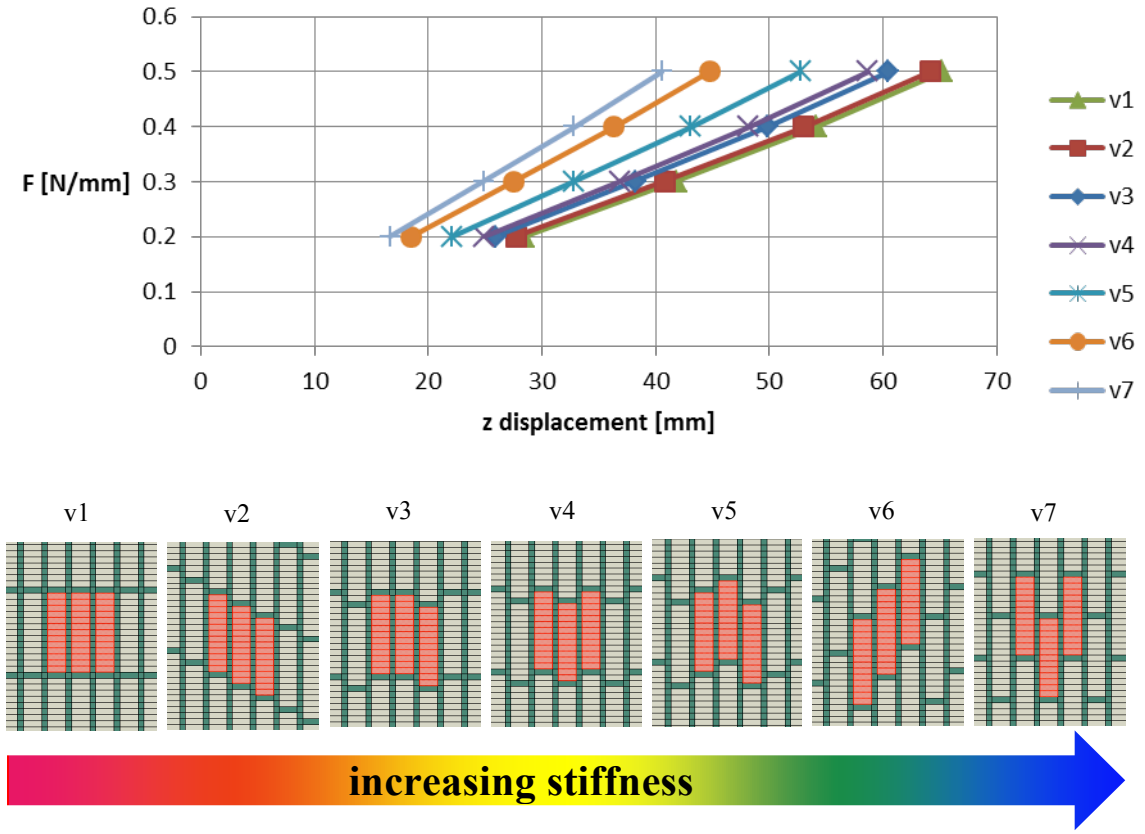

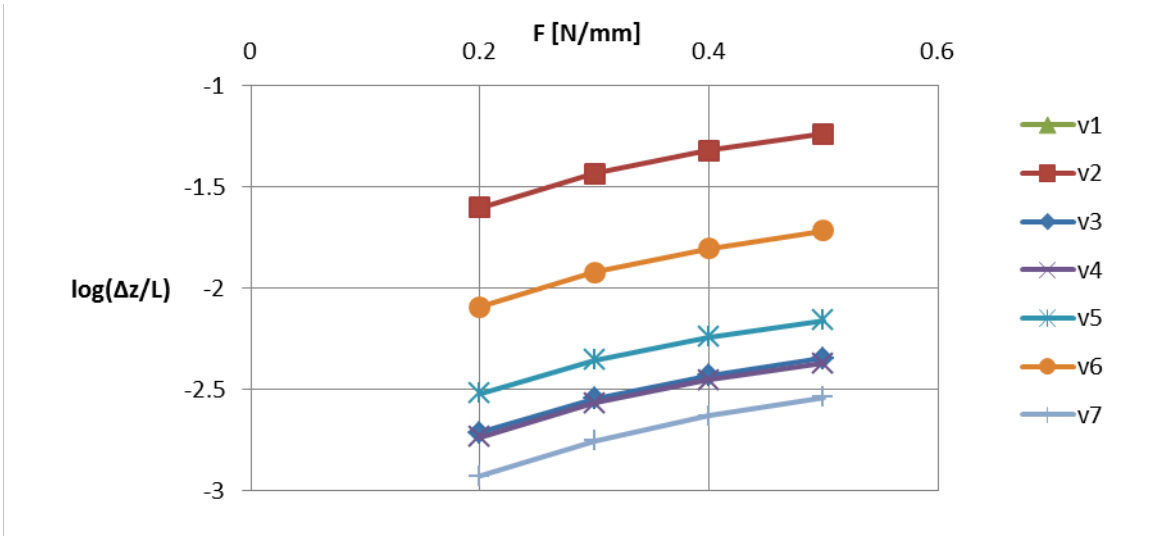

Figure 14 *On the first plot is represented the average of the two top corner z displacement by a given force applied on the upper edge of the model. The following diagram illustrates the three radial pattern ordered by increasing stiffness. Below, the plot display which geometry twists more with a given force showing the difference of the z displacement from the two upper corner over the depth of the model (L=144 mm).*

Figure 14 shows the different patterns, ordered by increasing stiffness. This order is given by the slope of the first plot in the same figure. This graphic must be interpreted as stress-

strain curve in the sense that we are using the gradient as a proxy of the stiffness in bending. It can be inferred that the closer and more aligned the joints are, the more compliant the structure is. A twisting of the top edge upon actuation would indicate that the wing is effectively anisotropic. The Δz between the corners is used as a measure of the twisting. v2 and v6 are the geometries where the twisting is relevant, where Δz is approximately 13% and 6%, respectively, related to average z displacement of the top edge. In the other cases, Δz is <2% of the average z displacement.

5.6 Stiffness parameters

The batoid's wing components can be arranged in different geometries, but looking at *Figure 8* and *Figure 11*, it seems that by taking the geometry defined as "v2" in the *Figure 14* and changing some parameters, we should be capable to model the radial and joint patterns of almost every part of the wing.

Material properties along the wing may vary depending on the amount of calcified cartilage of the radial. Material variables that can change in our model are the Young's modulus and Poisson's Ratio of both materials: E_{radial}, E_{joint}, ν_{radial}, and ν_{joint}. Nevertheless, we are going to keep them constant and focus on the geometric variables.

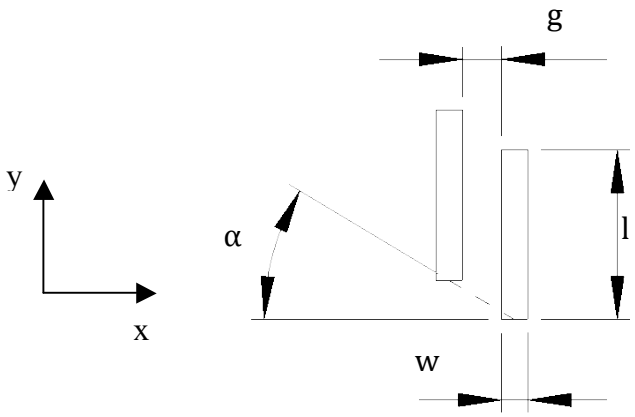

Figure 15 *Diagram representing the geometric parameters that may explain stiffness change.*

The geometric parameters which are believed to be responsible for the stiffness variation are the length, width, and thickness of the radial, represented by l, w, and t, respectively; the gap between two fin rays, i.e. the width of the joint, symbolized with g; and the offset between radials from neighboring fin rays, described as α.

In our research we are considering α and l changes while keeping constant the rest of parameters.

5.7 Results

5.7.1 Stiffness parameter: angle, α

Given the geometry defined on *Figure 12*, 8 angles were defined by changing the gap from 0.5 units to 4 between two joints of contiguous fin rays.

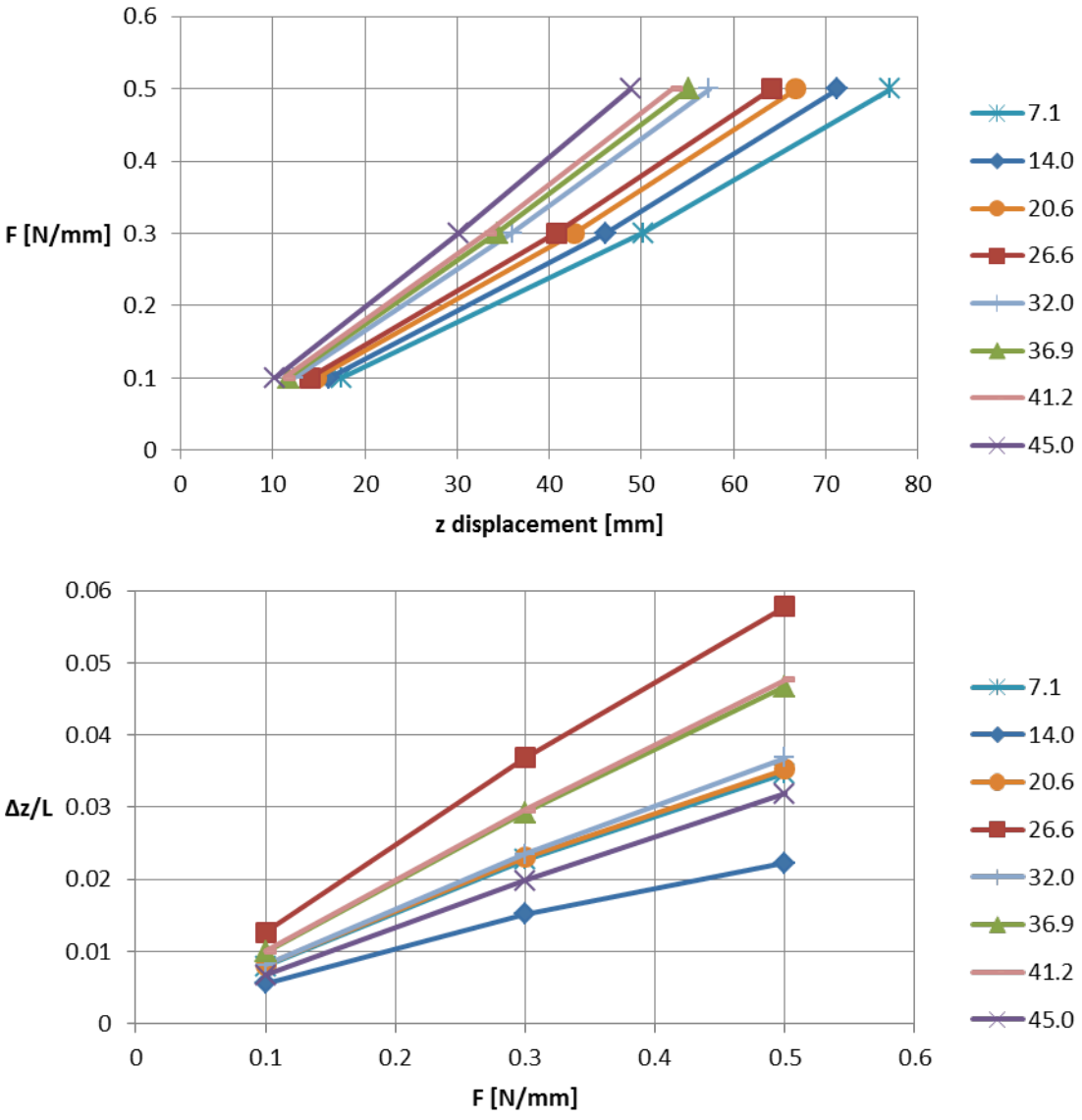

Figure 16 *Plot of the stiffness given by changing the angle.*

In this case an edge pulling force is applied, with magnitude between 0.1 N/mm to 0.5 N/mm. The average displacement between the two top corners and its difference over the length are represented in *Figure 16*. Again, they must be interpreted as a proxy of stiffness in bending and twisting, respectively.

As we would expect, the model becomes stiffer in bending when increasing the angle. On the other hand, there is not any clear trend in the twisting. Some other simulations (see [29]) were run to figure out what was happening, as significant twisting was expected from experimental evidence [4].

Given that the displacement increases linearly with the load, a single point (Z_0, F_0) gives us enough data compare one case to another. So, from now on, we will only be applying a load of 0.5 N/mm (Z_0, 0.5).

Although we attempted to make our model periodic, the choice of loadings and boundary conditions break the periodicity, as the model slightly changes depending on where the first joint is located. As this issue affects the results somewhat, we made 6 replicas of the same model, by sliding down one geometric element at a time (see *Figure 12*). Then, we plot the average displacement of each replica and its average for every angle presented before for an edge pulling force of 0.5 N/mm. We did the same for $\Delta z/L$ (*Figure 17*).

The bending plot shows clearly a visible linear trend from 14° to 45°. Again, the bending stiffness increases with the angle. It is important to remember that the stiffness is the slope of the straight line from each point to the origin. The particularities on the 0° and 7.1° are believed to be due to the connecting straight lines of joint existing on the model. We confirm that the non-periodicity of the model distorts the results but by taking the average of the replicas we can redress the effect of this systematic error.

Looking at twisting, the plot (*Figure 17*) does not show any clear trend. Having been proved experimentally an important twisting effect and the unsubstantial results from our model, we decided that $\Delta z/L$ was given us irrelevant information so we are not going to look at it anymore. That is probably because our model cannot capture twisting due to the lack of rotation degrees of freedom at the joints.

ETSEIB

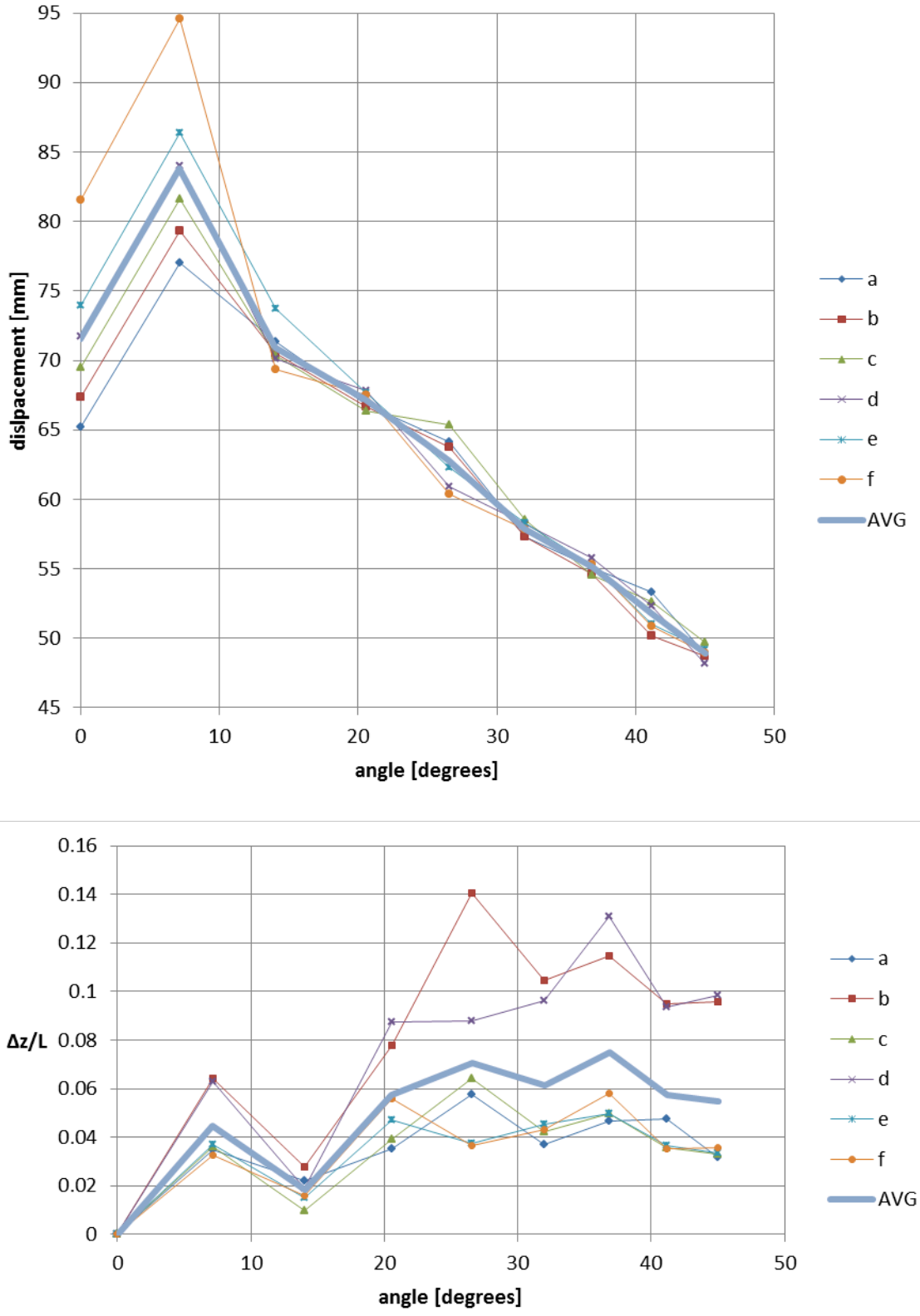

Figure 17 *Plot of the average displacement (indication of stiffness) and plot of the difference of the displacement of the corners (indication of twisting). 6 replicas and the average.*

5.7.2 Stiffness parameter: radial's length, l

Apart from the angle, *Figure 8* and *Figure 11* show that central radials are much longer than the ones near the edge. This is why we also simulated how the length affects the stiffness by a given angle. In this case, by taking the average of only two replicas, the trend seemed enough manifest.

Being the coefficient of determination >0.95 in all cases, it seems reasonable to confirm a linear trend between the radial length and the stiffness: when the radials decrease its length, the model becomes more compliant.

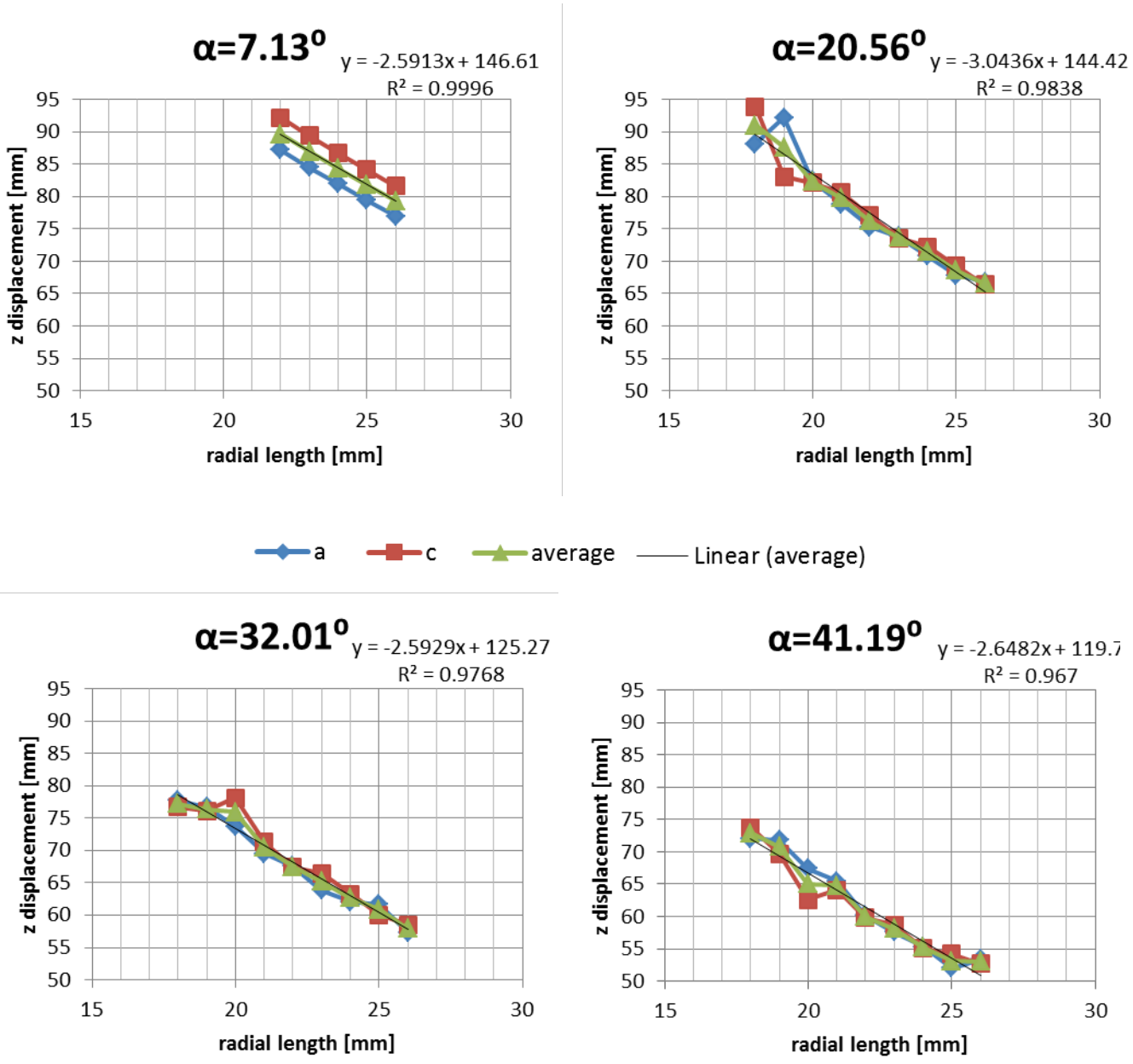

Figure 18 *Plot of the displacement for a 0.5 N/mm force at the top edge for different angles and radial lengths.*

5.8 Conclusions from the FEM analyses

Radial's length and offset, i.e. angle, have been demonstrated to be key factors on the stiffness of the model. Hence, given that the offset of the radials when the fin rays emanate from pectoral girdle is minute (*Figure 11*), the radials need to be long to provide the stiffness needed in this area, especially in oscillators.

In addition, some other simulations have been run with concentrated force on the top corners to find a trend on Δz but nothing has clearly emerged. Therefore, we conclude that our FE model is not sufficiently realistic to capture twisting of the wing upon edge loading.

Additionally, the results were excessively affected by the boundary conditions. To address this deficiency, we will attempt to build a new homogenized model to correct this effect, where no replicas will be necessary.

6 HOMOGENIZED MODEL

We are going to apply classic homogenization theory to calculate the effective in-plane elastic properties of the wing as a function of the geometry and materials properties of the radials and joints. A unit cell is defined and modeled with periodic boundary conditions. A MATLAB code written by E. Andreassen and C. S. Andreasen of Denmark Technical University was adopted for all calculations.

6.1 Methods

The stiffness matrix (or its inverse, the compliance matrix) fully characterizes the elastic response of a material. We are going to use numerical homogenization to determine the constants needed.

We are going to model the wing as a 6 mm thick laminate with a single ply. Hence, it will be under conditions of plane stress with all stress components in the out-of-plane direction being zero ($\sigma_3=\tau_{23}=\tau_{13}=0$). A representative volume element (RVE) will define the periodic unit cell.

The main function in the MATLAB code is called *homogenize*: its inputs are the width and height of the unit cell (l_x and l_y), two vectors with the first and second Lame's parameters for each material ($[\lambda_1\ \lambda_2]$ and $[\mu_1\ \mu_2]$), the angle Φ between the horizontal axis and the left wall in the unit cell, and a matrix **x**. The number of rows and columns equals the number of elements in the vertical and horizontal direction, respectively; and it determines the discretization. Each element of the matrix contains numbers 1 o 2 depending on the material of each mesh element [Andreassen E. and Andreassen C. S.].

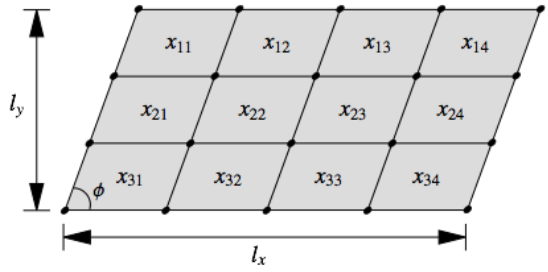

Figure 19 *Illustration of a mesh used to discretize a unit cell and its geometric parameters l_x, l_y and Φ [Andreassen E. and Andreassen C. S.].*

In our case, the RVE will always have l_y=28 mm but l_x will vary depending on how many fin rays are necessary to make the unit cell periodic.

The output of that function will be the $[Q]_{xy}$ matrix, being xy the same reference used on the FEA.

$$[Q]_{xy} = \begin{pmatrix} Q_{xx} & Q_{xy} & Q_{xs} \\ Q_{yx} & Q_{yy} & Q_{ys} \\ Q_{sx} & Q_{sy} & Q_{ss} \end{pmatrix} \quad (2)$$

By rotating the reference system using the [T] matrix, we will be able to determine which the stiff and compliant directions are.

$$[T] = \begin{pmatrix} m^2 & n^2 & 2mn \\ n^2 & m^2 & -2mn \\ -mn & mn & m^2 - n^2 \end{pmatrix} \quad (3)$$

where $m = \cos\theta$ and $n = \sin\theta$, and θ is the rotation angle. The new stiffness matrix $[Q]_{12}$ can be written in an arbitrary reference system (x_1,x_2) as:

$$[Q]_{12} = [T][Q]_{xy}[T]^{-1} \quad (4)$$

By maximizing and minimizing the first element of the matrix (Q_{11}) in function of the angle θ, we are going to find the reference system such that the 1 axis is the stiff and compliant direction, respectively.

$$Q_{11} = m^4 Q_{xx} + n^4 Q_{yy} + m^2 n^2 (2Q_{xy} + 4Q_{ss}) + 4m^3 n Q_{xs} + 4mn^3 Q_{ys} \quad (5)$$

This will provide an indication of the anisotropy of the wing.

6.2 **Results**

The calculations have been repeated for 4 different angles with the same mesh used in de FEA. Within them, we have analyzed the stiffer efficacy of the cross braces (*Figure 21)* and we have distinguished between two cases. The first one has only horizontal connections between radials from contiguous fin rays, whereas the second also features vertical connections between radials from the same fin ray. In both cases, the connections are considered with the same material properties as the radials. Indeed, the connections are uncalcified cartilage surrounded by tesserae, just like radials.

ETSEIB

However, the lower angle case (α=14.04°) doesn't have the possibility of stiffening the wing using cross braces because of geometric incompatibility: i.e., it doesn't have enough space because the offset is too small. cartilage surrounded by tesserae, just like radials.

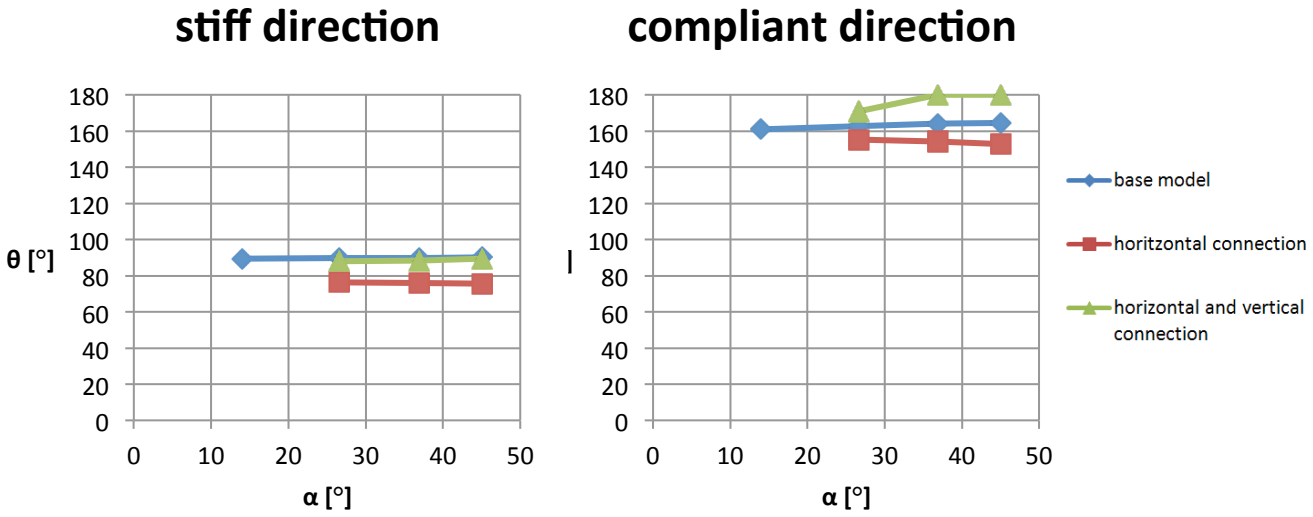

Figure 20 *Plot of the stiff and compliant direction. Angle α is the offset between radials of contiguous fin rays and θ is the angle between x direction (Figure 15) and the stiff and compliant direction, respectively; defined positive CCW.*

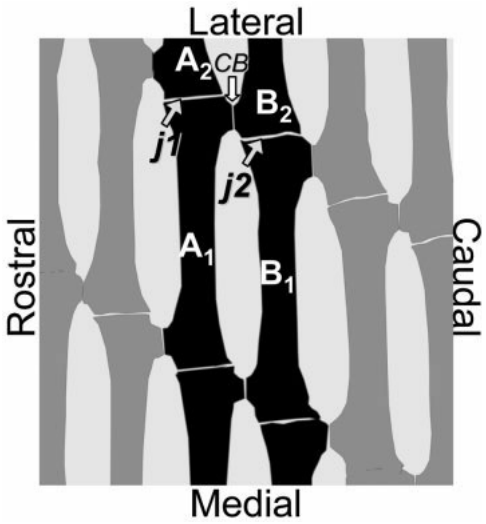

Figure 21 *Schematic of cross-bracing. Fin ray "A" is joined to fin ray "B" by a cartilaginous extension (CB). This inhibits the bending of normal radial joints j1 and j2. When the joint between radials B1 and B2 tries to bend, radial A1 will be forced to bend along with them, effectively eliminating the ability of j2 to bend. These cross-braces are arranged in diagonal patterns such that the entire area is reinforced and stiffened [28].*

Where α is the offset angle between radials of adjacent fin rays (*Figure 15*) and θ orients stiff and compliant direction, respectively; CCW from the x axis (*Figure 15*). That is, the directions on which the pulling force need to be higher and lower to achieve deformation given.

Looking and comparing the reduced stiffness $[Q]_{xy}$ of the base model, only horitzontal connection model and both horizontal and vertical connection model; we can get a sense on how cross braces stiffen our model (*Figure 22*). Moreover, we can guess if the stiffening is higher on the x or y-direction depending if the term which increases more is Q_{xx} or Q_{yy}.

	base model	**horizontal connection**	**horizontal and vertical connection**
α=14.04°	$\begin{pmatrix} 106.21 & 14.85 & 0 \\ 14.85 & 313.37 & 3.08 \\ 0 & 3.08 & 33.25 \end{pmatrix}$	-	-
α=26.57°	$\begin{pmatrix} 106.22 & 15.40 & -0.02 \\ 15.40 & 331.30 & 1.69 \\ -0.02 & 1.69 & 34.27 \end{pmatrix}$	$\begin{pmatrix} 139.39 & 57.82 & 26.08 \\ 57.82 & 630.65 & 117.48 \\ 26.08 & 117.48 & 82.68 \end{pmatrix}$	$\begin{pmatrix} 219.8 & 77.1 & 8.6 \\ 77.1 & 1697.8 & 54.2 \\ 8.6 & 54.2 & 9.02 \end{pmatrix}$
α=36.87°	$\begin{pmatrix} 106.22 & 15.71 & -0.02 \\ 15.71 & 346.01 & 0.82 \\ -0.02 & 0.82 & 34.71 \end{pmatrix}$	$\begin{pmatrix} 149.09 & 57.33 & 26.71 \\ 57.33 & 622.44 & 117.36 \\ 26.71 & 117.36 & 86.32 \end{pmatrix}$	$\begin{pmatrix} 217.3 & 79.0 & -1.7 \\ 79.0 & 1676 & 46.6 \\ 79.4 & 46.6 & 102.1 \end{pmatrix}$
α=45.00°	$\begin{pmatrix} 106.23 & 15.93 & -0.02 \\ 15.93 & 357.50 & 0.27 \\ -0.02 & 0.27 & 34.91 \end{pmatrix}$	$\begin{pmatrix} 161.00 & 55.43 & 27.00 \\ 55.43 & 609.96 & 116.64 \\ 27.00 & 116.64 & 90.31 \end{pmatrix}$	$\begin{pmatrix} 226.2 & 86.9 & -13.9 \\ 86.9 & 1682.2 & 32.9 \\ -13.9 & 32.9 & 119.9 \end{pmatrix}$

Figure 22 *Table with the reduced stiffness matrix $[Q]_{xy}$ using a homogenized model.*

6.3 Conclusions from the homogenized model

Looking at the reduced stiffness matrices, the diagonal terms doesn't change much when increasing the angle α; this result is not consistent with our FEA predictions. However, in that case we were defining out of plane loads which caused deformation out of plane.

ETSEIB

The cross braces certainly play a key role on the stiffening of the wing. Looking at the Q matrices, the diagonal terms, especially $Q_{22,}$ change dramatically. When pulling in the x direction, while in the base model there are complete layer of compliant material (i.e. joint) and this is essentially what stretches, in both cross braces model there are radial 'inserts' which decreases this stretching.

The stiff and complaint direction barely change when varying angle α. Having the conviction that in an actual wing by changing the principal directions of a small part of the wing the animal can swim more efficiently, we conclude that the connections between radials are not rigorous enough in our model. Thus, a 3D model should be used to explain the twisting.

7 CONCLUSIONS AND FUTURE WORK

Batoid fishes are surely a unique inspiration source for the development of what will be the next generation of AUVs. Mimicking their advantageous morphological features will results in new designs that outperform traditional propeller systems. Many prototypes have been demonstrated during the last decade but, although most of them success in mimicking the undulatory or oscillatory swimming style, lot of works need to be done to build a truly bio-inspired AUV. To this end, the first step that we decided to pursue in this work is to understand the relationship between the morphology of the wing and its elastic properties.

After defining a computational model with the geometry and material properties of a batoid wing, a Finite Element Analysis using ABAQUS has been carried out. Different parameters believed responsible of the batoid wing stiffness have been explored. The batoid wing becomes locally stiffer by making the radials shorter or increasing the offset between radials of contiguous fin rays, i.e. increasing l or α. By keeping every variable constant but changing where the joints were located we found more discrepancy than expected. That is why some replicas were run and the average was taken as a final result for the FEA.

Another numeric approach to extract the effective material properties of the wing as function of its geometric parameters was investigated, using numerical homogenization. Using a MATLAB code written by by E. Andreassen and C. S. Andreasen of Denmark Technical University, we were able to find the stiff and compliant direction of wings as well as their reduced stiffness matrix [Q]. These directions remained almost constant when changing α. That suggests that the wing behavior is not properly captured by our 2D model.

Consequently, further research needs to be done using a 3D model which should capture better the connections between radials. Most likely, a torsional degree of freedom at the joints (not modeled in this work) is responsible for the observed behavior. Maybe the joints should be considered stiffer when the radials belong to the same fin ray and adding a third material representing the mix of connective tissue and muscles could be a good starting point. Also the joints can be studied and thus modeled more realistically. During

all this process, it would be a good idea to have a real prototype to predict the results expected from each simulation. This prototype could be easily assembled using rapid prototyping techniques available at UCI, such as 3D printing and stereolithography.

ACKNOWLEDGMENTS

I would like to express my sincere gratitude to my advisor, Professor Lorenzo Valdevit, for his supervision, support and continuous encouragement.

Moreover, I would like to sincerely thank Professor Justin Schaefer for sharing with us his biological knowledge of the batoid fishes and his valuable help.

Also, thanks to my lab-mates and Catalan students at UCI who created a pleasant environment for working and have fun when needed. In addition, I would like to acknowledge Roger Rangel for his efforts and work for the Catalan community at UCI.

Finally, I would like to acknowledge the financial support from the Balsells fellowship.

REFERENCES

[1] Alvarado, P., Chin, S., Larson, W., Mazumdar, A., Toumi, K., "A soft body under-actuated approach to multi degree of freedom biomimetic robots: A stingray example". *3rd IEEE RAS and EMBS International Conference*, Tokyo, 2010, 473–478.

[2] Boileau, R., Fan, L., Moore, T., "Mechanization of Rajiform Swimming Motion: The Making of Robot-ray". *Engineering Physics Project Laboratory, Applied Science* 479 Final Report, Project Number 0159, University of British Columbia, 2002

[3] Cai, Y., Bi, S., Liege, Z., Gao, J., "Design of a robotic fish propelled by oscillating flexible pectoral foils". *International Conference on Intelligent Robots and System,St. Louis, Mo, US,* 2138-42, 2009.

[4] Carreira, E., Valdevit, L., "Mechanical Investigation of a Novel Bio-Mimetic Morphing Structure", University of California Irvine, 2009

[5] De Carvalho, M.R., Maisey, J.G., Grande, L., "Freshwater stingrays of the Green River Formation of Wyoming (early Eocene), with the description of a new genus and species and an analysis of its phylogenetic relationships (chondrichthyes: myliobatiformes)". *Bull Am Mus Nat Hist* 284:1–136, 2004.

[6] Clark, R. P., Smits, A. J., "Thrust production and wake structure of a Batoid-inspired oscillating fin". *Journal of Fluid Mechanics*, 562, 415–429, 2006.

[7] Compagno, L. J.V., "Phyletic relationships of living sharks and rays". *Am Zool* 17:303–322, 1977.

[8] Compagno, L. J. V., "Systematics and body form". In *Sharks, Skates and Rays: The Biology of Elasmobranch Fishes* (ed. W. C. Hamlett), pp. 1–42. Baltimore, MD: John Hopkins University Press, 1999.

[9] Dean, M.N., Summers, A.P., "Mineralized cartilage in the skeleton of chondrichthyan fishes". *Zoology* (Jena) 109, 164–168, 2006.

[10] Fish, F. E., "Biomimetics: Determining engineering opportunities from nature". *Proceedings SPIE Conference, SPIE* Vol. 7401, 740109, 2009.

[11] Fish, F. E., Koack, D. M., "Biomimetics and Marine Technology: An introduction". Marine Technology Society Journal 45(4): 8-13, 2011.

[12] Fish, F. E., Weber, P. W., Murray, M. M., and Howle, L. E., "Marine applications of the biomimetic humpback whale flipper". *Marine Technology Society Journal* 45(4): 198-207, 2011.

ETSEIB

[13] Gao, J., Bi, S., Li, J., Cong, L., "Design and experiments of robot fish propelled by pectoral fins". *Proceedings of the IEEE International Conference on Robotics and Biomimetics, Guilin, China,* 445-50, 2009.

[14] Geder, J., Palmisano, J., Ramamurti, R., Sandberg, W. C., Ratna, B., "Fuzzy logic PID based control design and performance for a pectoral fin propelled unmanned underwater vehicle". *Proceedings of the International Conference on Control*, *Automation and Systems*, Seoul, South Korea, 40–46, 2008.

[15] Henak, C.R., Anderson, A.E., Weiss, J.A., "Subject-Specific Analysis of Joint Contact Mechanics: Application to the Study of Osteoarthritis and Surgical Planning". *J Biomech Eng.* ;135(2):021003-021003-26. doi:10.1115/1.4023386, 2013.

[16] Liem, K.F., Summers, A.P., "Muscular system: gross anatomy and functional morphology of muscles"; in *Hamlett WC* (ed): Sharks, Skates and Rays. The Biology of Elasmobranch Fishes. Baltimore, John Hopkins Press, pp 93–114, 1999.

[17] Liu, X., Dean, M.N., Summers, A.P., Earthman, J.C., "Composite model of shark's skeleton in bending: A novel architecture for biomimetic design of functional compression bias". *Materials Science and Engineering: C*, 30, 1077-1084, 2010.

[18] Low, K. H., Prabu, S., Yang, J., Zhang, S. W., Zhang, Y. H., "Design and initial testing of a single-motor-driven spatial pectoral fin mechanism". *International Conference on Mechatronics and Automation*, Harbin, China, 503–508, 2007.

[19] Low, K. H., "Modelling and parametric study of modular undulating fin rays for fish robots". *Mechanism and Machine Theory*, 44, 615–632, 2009.

[20] Macesic, L. J., Summers, A. P., "Flexural stiffness and composition of the batoid propterygium as predictors of punting ability". *J. Exp. Biol.* 215, 2003- 2012, 2012.

[21] McKenna, TM., "Developing Bioinspired Autonomous Systems". *Marine Technology Society Journal* Volume: 45 Issue: 4 Pages: 19-23 COLUMBIA, MD 21044 USA, 2011.

[22] Moored, K. W., Fish, F. E., Kemp, T. H. and Bart-Smith, H., "Batoid fishes: inspiration for the next generation of underwater robots". *Marine Technology Society Journal* 45(4): 99-109, 2011.

[23] Niu, C., Zhang, L., Bi, S., Yueri, C., "Development and depth control of a robotic fish mimicking cownose ray". *Proceedings of the IEEE International Conference on Robotics and Biomimetics, Guangzhou, China,* 814-18, 2012.

[24] Porter, M. E., Beltran, J. L., Koob, T. J. and Summers, A. P., "Material properties and biochemical composition of mineralized vertebral cartilage in seven elasmobranch species (Chondrichthyes)". *J Exp Biol* 209, 2920-2928, 2006.

[25] Punning, A., Anton, M., Kruusmaa, M., Aabloo, A., "A biologically inspired ray-like underwater robot with electroactive polymer pectoral fins". *Proceedings of the IEEE International Conference on Mechatronics and Robotics*, Aachen, German, 2, 241–245, 2004.

[26] Rosenberger, L.J., Westneat, M.W., "Functional morphology of undulatory pectoral fin locomotion in the stingray *Taeniura lymma* (Chondrichthyes: Dasyatidae)". *J Exp Biol* 202:3523–3539, 1999.

[27] Rosenberger, L. J., "Pectoral fin locomotion in batoid fishes: undulation versus oscillation". *J. Exp. Biol*. 204, 379-394, 2001.

[28] Schaefer, J.T., Summers, A.P., "Batoid wing skeletal structure: novel morphologies, mechanical implications, and phylogenetic patterns". *J. Morphol*. 264, 298–313, 2005.

[29] Schaefer, J.T., "Mechanical Implications of Joint Location in Batoid Pectoral Fins", 2007.

[30] Sfakiotakis, M., Lane, D. M., Davies B. C., "An experimental undulating-fin device using the parallel bellows actuator". *Proceedings of the IEEE International Conference on Robotics & Automation*, Seoul, Korea, 2356–2362, 2001.

[31] Takagi, K., "Development of a rajiform swimming robot using ionic polymer artificial muscles". *Proceedings of the IEEE/RSJ International Conference on Intelligent Robots and Systems*, San Diego, California, USA, 1861–1866, 2006.

[32] Tangorra, J., Anquetil, P., Fofonoff, T., Chen, A., Zio, M. D., Hunter, I., "The application of conducting polymers to a biorobotic fin propulsor". *Bioinspiration & Biomimetics*, 2, S6–S17, 2007.

[33] Webb, P. W., "The biology of fish swimming". In *Mechanics and Physiology of Animal Swimming* (ed. L. Maddock, Q. Bone and J. M. V. Rayner), pp. 45–62. Cambridge: Cambridge University Press, 1994.

[34] Yang, S. B., Qiu, J., Han, X. Y., "Kinematics modeling and experiments of pectoral oscillation propulsion robotic fish". *Journal of Bionic Engineering*, 6, 174–179, 2009.

[35] Zhang, Y., He, J., Low, K. H., "Parametric study of an underwater finned propulsor inspired by bluespotted ray". *Journal of Bionic Engineering*, 9, 166–176, 2012.

Websites:

ETSEIB

[36] Mantabot-the next generation sea-robot. *The future of things*. Retrieved 2 September 2013, from http://thefutureofthings.com/news/11486/mantabot-the-next-generation-sea-robot.html

[37] Southern tingray. [Photograph]. *Encyclopedia Britannica Online*. Retrieved 25 June 2013, from http://www.Britannica.com/EBchecked/media/92147/Southern-stingrays

ANNEX A: ABAQUS SCREENSHOTS

A.1 Geometries from the preliminary results

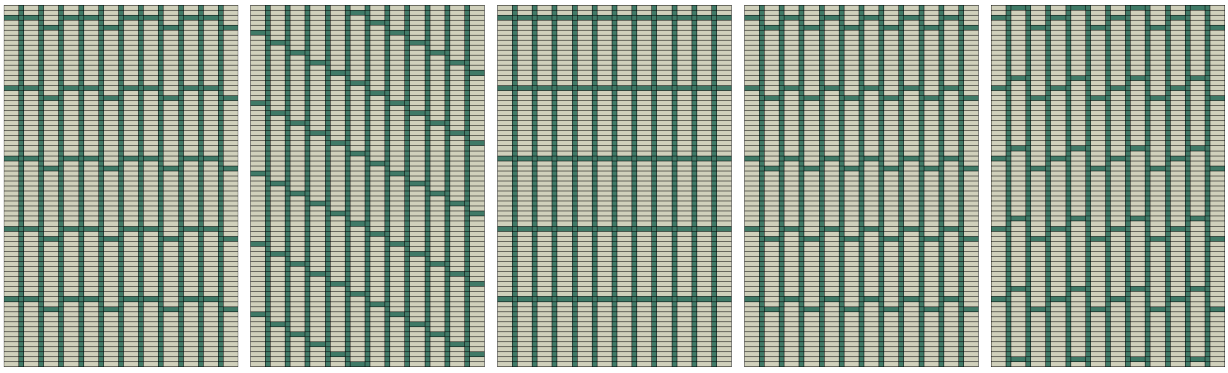

v1 v2 v3 v4 v5

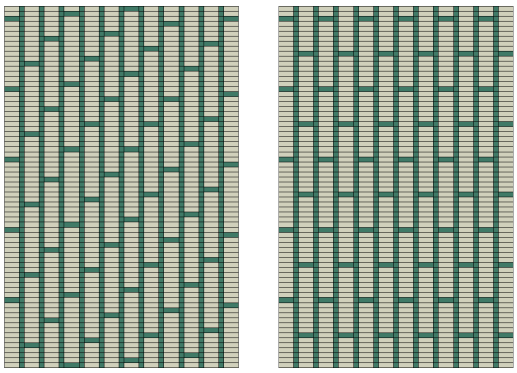

v6 v7

A.2 Boundary Conditions

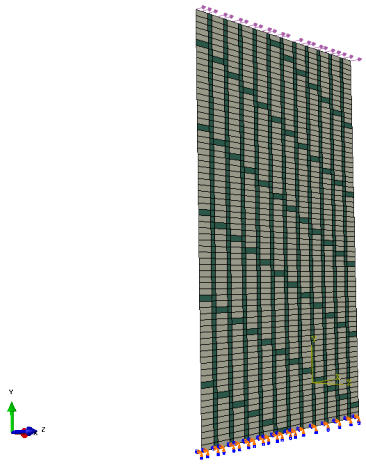

A.3 Mesh

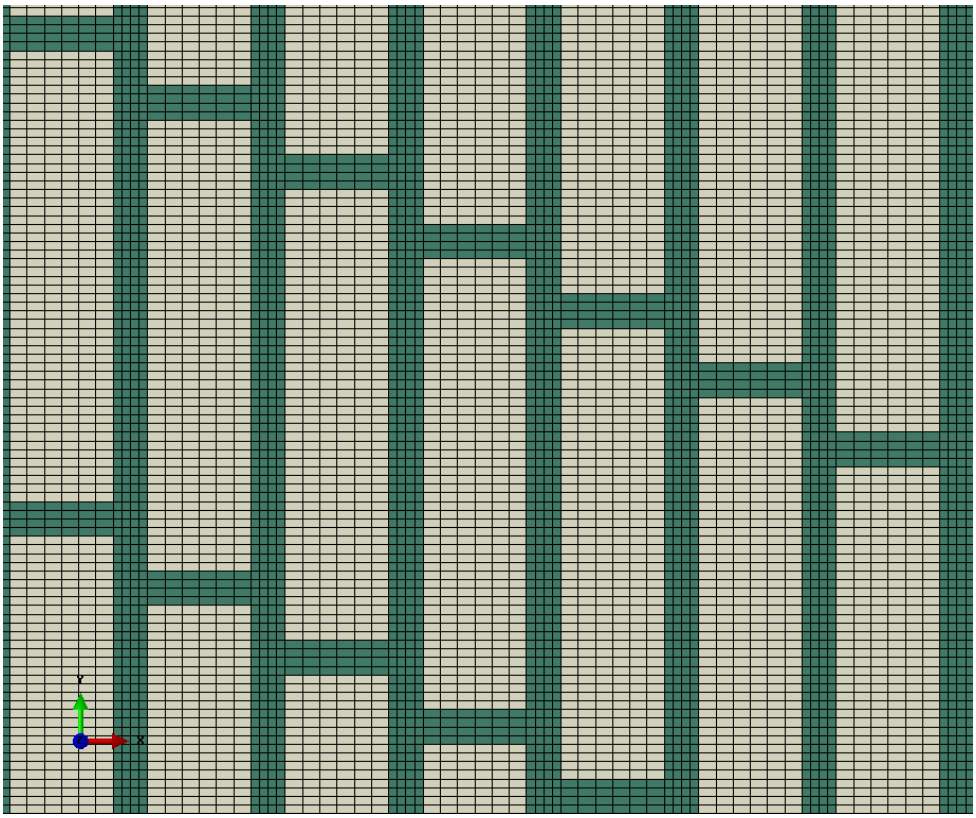

A.4 α=26.6°, l=26mm replicas

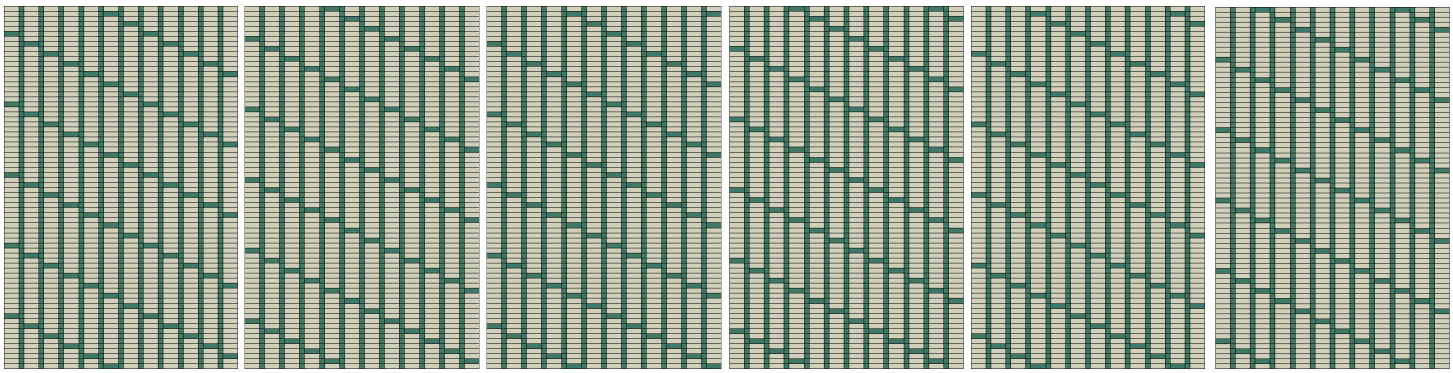

A.5. Von Misses stress plot α=45.0°, l=26mm, edge pulling force 0.5 N/mm.

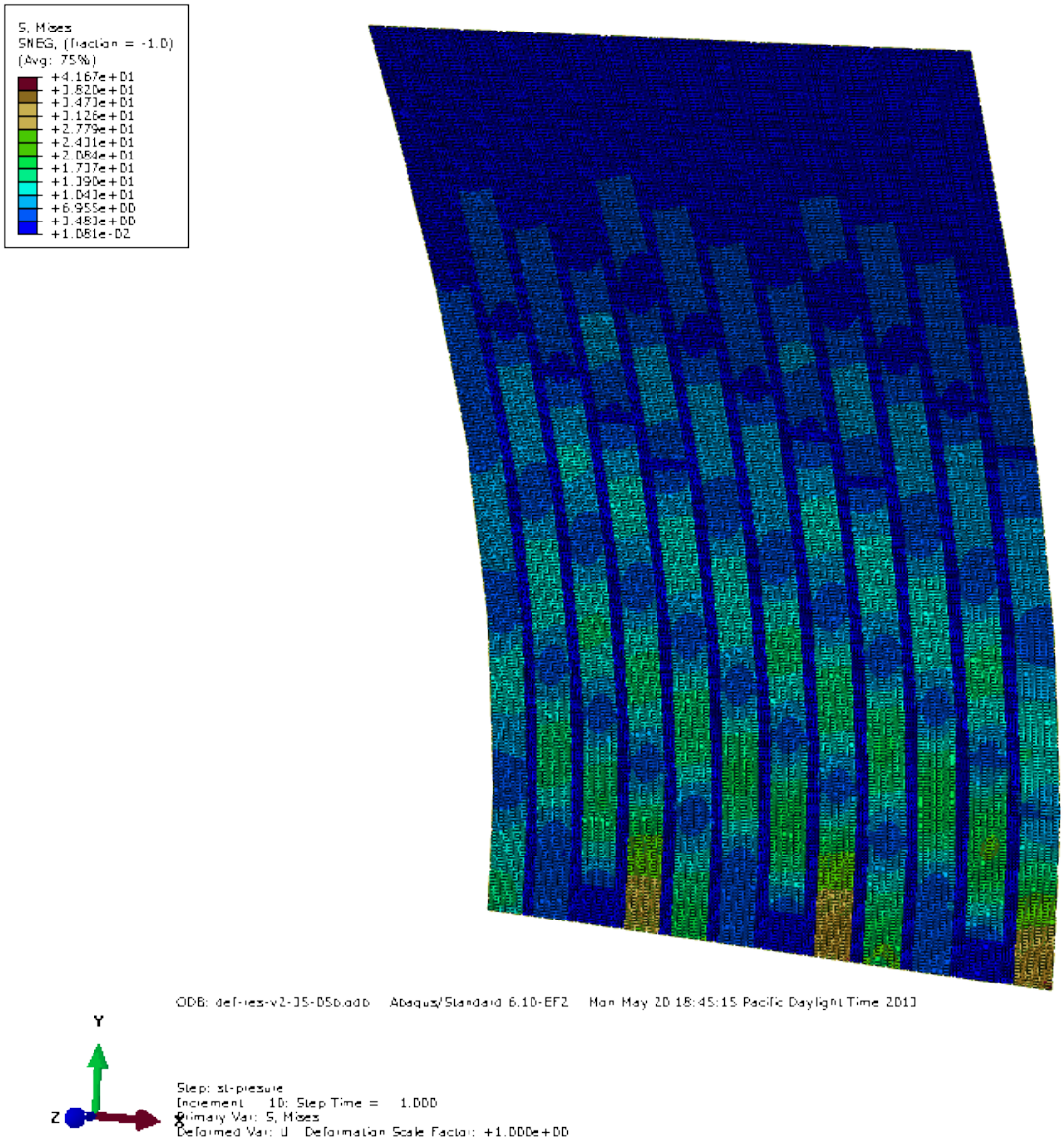

ANNEX B: MATLAB CODE

B.1 Homogenization

```
function [CH,Y,alphas,alphaw] = homogenize(lx, ly, lambda, mu, phi, x)
%%%%%%%%%%%%%%%%%%%%%%%%%%%%%%%%%%%%%%%%%%%%%%%%%%%%%%%%%%%%%%%%%%%%%%%%%%%%
% lx = Unit cell length in x-direction.
% ly = Unit cell length in y-direction.
% lambda = Lame's first parameter for both materials. Two entries.
% mu = Lame's second parameter for both materials. Two entries.
% phi = Angle between horizontal and vertical cell wall. Degrees
% x = Material indicator matrix. Size used to determine nelx/nely
%%%%%%%%%%%%%%%%%%%%%%%%%%%%%%%%%%%%%%%%%%%%%%%%%%%%%%%%%%%%%%%%%%%%%%%%%%%%
%% INITIALIZE
% Deduce discretization
[nely, nelx] = size(x);
% Stiffness matrix consists of two parts, one belonging to lambda and
% one belonging to mu. Same goes for load vector
dx = lx/nelx; dy = ly/nely;
nel = nelx*nely;
[keLambda, keMu, feLambda, feMu] = elementMatVec(dx/2, dy/2, phi);
% Node numbers and element degrees of freedom for full (not periodic) mesh
nodenrs = reshape(1:(1+nelx)*(1+nely),1+nely,1+nelx);
edofVec = reshape(2*nodenrs(1:end-1,1:end-1)+1,nel,1);
edofMat = repmat(edofVec,1,8)+repmat([0 1 2*nely+[2 3 0 1] -2 -1],nel,1);
%% IMPOSE PERIODIC BOUNDARY CONDITIONS
% Use original edofMat to index into list with the periodic dofs
nn = (nelx+1)*(nely+1); % Total number of nodes
nnP = (nelx)*(nely); % Total number of unique nodes
nnPArray = reshape(1:nnP, nely, nelx);
% Extend with a mirror of the top border
nnPArray(end+1,:) = nnPArray(1,:);
% Extend with a mirror of the left border
nnPArray(:,end+1) = nnPArray(:,1);
% Make a vector into which we can index using edofMat:
dofVector = zeros(2*nn, 1);
dofVector(1:2:end) = 2*nnPArray(:)-1;
dofVector(2:2:end) = 2*nnPArray(:);
edofMat = dofVector(edofMat);
ndof = 2*nnP; % Number of dofs
%% ASSEMBLE STIFFNESS MATRIX
% Indexing vectors
iK = kron(edofMat,ones(8,1))';
jK = kron(edofMat,ones(1,8))';
% Material properties in the different elements
lambda = lambda(1)*(x==1) + lambda(2)*(x==2);
mu = mu(1)*(x==1) + mu(2)*(x==2);
% The corresponding stiffness matrix entries
sK = keLambda(:)*lambda(:).' + keMu(:)*mu(:).';
K = sparse(iK(:), jK(:), sK(:), ndof, ndof);
%% LOAD VECTORS AND SOLUTION
% Assembly three load cases corresponding to the three strain cases
sF = feLambda(:)*lambda(:).'+feMu(:)*mu(:).';
iF = repmat(edofMat',3,1);
jF = [ones(8,nel); 2*ones(8,nel); 3*ones(8,nel)];
F = sparse(iF(:), jF(:), sF(:), ndof, 3);
% Solve (remember to constrain one node)
chi(3:ndof,:) = K(3:ndof,3:ndof)\F(3:ndof,:);
%% HOMOGENIZATION
% The displacement vectors corresponding to the unit strain cases
chi0 = zeros(nel, 8, 3);
% The element displacements for the three unit strains
chi0_e = zeros(8, 3);
ke = keMu + keLambda; % Here the exact ratio does not matter, because
fe = feMu + feLambda; % it is reflected in the load vector
chi0_e([3 5:end],:) = ke([3 5:end],[3 5:end])\fe([3 5:end],:);
% epsilon0_11 = (1, 0, 0)
chi0(:,:,1) = kron(chi0_e(:,1)', ones(nel,1));
% epsilon0_22 = (0, 1, 0)
```

ETSEIB

```
chi0(:,:,2) = kron(chi0_e(:,2)', ones(nel,1));
% epsilon0_12 = (0, 0, 1)
chi0(:,:,3) = kron(chi0_e(:,3)', ones(nel,1));
CH = zeros(3);
cellVolume = lx*ly;
for i = 1:3
for j = 1:3
sumLambda = ((chi0(:,:,i) - chi(edofMat+(i-1)*ndof))*keLambda).*...
(chi0(:,:,j) - chi(edofMat+(j-1)*ndof));
sumMu = ((chi0(:,:,i) - chi(edofMat+(i-1)*ndof))*keMu).*...
(chi0(:,:,j) - chi(edofMat+(j-1)*ndof));
sumLambda = reshape(sum(sumLambda,2), nely, nelx);
sumMu = reshape(sum(sumMu,2), nely, nelx);
% Homogenized elasticity tensor
CH(i,j) = 1/cellVolume*sum(sum(lambda.*sumLambda + mu.*sumMu));
end
end
disp('--- Homogenized elasticity tensor ---'); disp(CH)
% STIFF AND COMPLIANT DIRECTION
Qxx=CH(1,1);
Qyy=CH(2,2);
Qss=CH(3,3);
Qxy=CH(1,2);
Qxs=CH(1,3);
Qys=CH(2,3);
alphas=fminbnd(@(alphas) Q11s(alphas,Qxx,Qyy,Qss,Qxy,Qxs,Qys),0,pi);
alphaw=fminbnd(@(alphaw) Q11w(alphaw,Qxx,Qyy,Qss,Qxy,Qxs,Qys),0,pi);
disp('--- Stiffest direction ---'); disp(radtodeg(alphas))
disp('--- Weakest direction ---'); disp(radtodeg(alphaw))
% COMPLIANCE MATRIX
Y=inv(CH);
disp('--- S matrix ---'); disp(Y)

%% COMPUTE ELEMENT STIFFNESS MATRIX AND FORCE VECTOR (NUMERICALLY)
function [keLambda, keMu, feLambda, feMu] = elementMatVec(a, b, phi)
% Constitutive matrix contributions
CMu = diag([2 2 1]); CLambda = zeros(3); CLambda(1:2,1:2) = 1;
% Two Gauss points in both directions
xx=[-1/sqrt(3), 1/sqrt(3)]; yy = xx;
ww=[1,1];
% Initialize
keLambda = zeros(8,8); keMu = zeros(8,8);
feLambda = zeros(8,3); feMu = zeros(8,3);
L = zeros(3,4); L(1,1) = 1; L(2,4) = 1; L(3,2:3) = 1;
for ii=1:length(xx)
for jj=1:length(yy)
% Integration point
x = xx(ii); y = yy(jj);
% Differentiated shape functions
dNx = 1/4*[-(1-y) (1-y) (1+y) -(1+y)];
dNy = 1/4*[-(1-x) -(1+x) (1+x) (1-x)];
% Jacobian
J = [dNx; dNy]*[-a a a+2*b/tan(phi*pi/180) 2*b/tan(phi*pi/180)-a; ...
-b -b b b]';
detJ = J(1,1)*J(2,2) - J(1,2)*J(2,1);
invJ = 1/detJ*[J(2,2) -J(1,2); -J(2,1) J(1,1)];
% Weight factor at this point
weight = ww(ii)*ww(jj)*detJ;
% Strain-displacement matrix
G = [invJ zeros(2); zeros(2) invJ];
dN = zeros(4,8);
dN(1,1:2:8) = dNx;
dN(2,1:2:8) = dNy;
dN(3,2:2:8) = dNx;
dN(4,2:2:8) = dNy;
B = L*G*dN;
% Element matrices
keLambda = keLambda + weight*(B' * CLambda * B);
keMu = keMu + weight*(B' * CMu * B);
% Element loads
feLambda = feLambda + weight*(B' * CLambda * diag([1 1 1]));
feMu = feMu + weight*(B' * CMu * diag([1 1 1]));
```

ETSEIB

```
end
end

% STIFF DIRECTION
function f=Q11s(alphas,Qxx,Qyy,Qss,Qxy,Qxs,Qys)
f=(-1)*((cos(alphas))^4*Qxx+(sin(alphas))^4*Qyy+(cos(alphas))^2*(sin(alphas))^2*
(2*Qxy+4*Qss)+4*(cos(alphas))^3*sin(alphas)*Qxs+4*cos(alphas)*(sin(alphas))^3*Qys);

% COMPLIANT DIRECTION
function f=Q11w(alphaw,Qxx,Qyy,Qss,Qxy,Qxs,Qys)
f=(cos(alphaw))^4*Qxx+(sin(alphaw))^4*Qyy+(cos(alphaw))^2*(sin(alphaw))^2*
(2*Qxy+4*Qss)+4*(cos(alphaw))^3*sin(alphaw)*Qxs+4*cos(alphaw)*(sin(alphaw))^3*Qys;
```

B.2 Assign material properties

B.2.1 Lamé's first parameter (λ):

```
function [ lambda ] = assignlambda( E1, E2, nu1, nu2 )
%assignlambda Calculates lambda vector for 2 materials
lambda1=lame_lambda( E1, nu1 );
lambda2=lame_lambda( E2, nu2 );
mu1=lame_mu( E1, nu1 );
mu2=lame_mu( E2, nu2 );
lambda1= lambda_mod( lambda1, mu1 );
lambda2= lambda_mod( lambda2, mu2 );
lambda=[lambda1 lambda2];
end

function [ lambda ] = lame_lambda( E, nu )
% lame_lambda Calculates first Lame's parameter lambda
lambda=(nu*E)/((1.+nu)*(1.-2.*nu));
end

function [ mu ] = lame_mu( E, nu )
% lame_mu Calculates second Lame's parameter mu
mu=E/(2*(1+nu));
end

function [ lambdam ] = lambda_mod( lambda, mu )
% lambda_mod Calclates modified Lamé's first parameter to get plane
stress properties
lambdam=2*mu*lambda/(lambda+2.*mu);
end
```

B.2.2 Lame's second parameter (μ):

```
function [ mu ] = assignmu( E1,E2,nu1,nu2 )
%assignmu Calculates mu vector for 2 materials
mu1=lame_mu( E1, nu1 );
mu2=lame_mu( E2, nu2 );
mu=[mu1 mu2];
end
```

ETSEIB

```
function [ mu ] = lame_mu( E, nu )
% lame_mu Calculates second Lame's parameter mu
end
```

B.3 Example of and x matrix (base model α=26.57°):

2	1	1	1	2	1	1	1	2	1	1	1	2	1	1	1	2	1	1	1	2	1	1	1	2	1	1	1
2	2	2	2	2	1	1	1	2	1	1	1	2	1	1	1	2	1	1	1	2	1	1	1	2	1	1	1
2	1	1	1	2	1	1	1	2	1	1	1	2	1	1	1	2	1	1	1	2	1	1	1	2	1	1	1
2	1	1	1	2	2	2	2	2	1	1	1	2	1	1	1	2	1	1	1	2	1	1	1	2	1	1	1
2	1	1	1	2	1	1	1	2	1	1	1	2	1	1	1	2	1	1	1	2	1	1	1	2	1	1	1
2	1	1	1	2	1	1	1	2	2	2	2	2	1	1	1	2	1	1	1	2	1	1	1	2	1	1	1
2	1	1	1	2	1	1	1	2	1	1	1	2	1	1	1	2	1	1	1	2	1	1	1	2	1	1	1
2	1	1	1	2	1	1	1	2	1	1	1	2	2	2	2	2	1	1	1	2	1	1	1	2	1	1	1
2	1	1	1	2	1	1	1	2	1	1	1	2	1	1	1	2	1	1	1	2	1	1	1	2	1	1	1
2	1	1	1	2	1	1	1	2	1	1	1	2	1	1	1	2	2	2	2	2	1	1	1	2	1	1	1
2	1	1	1	2	1	1	1	2	1	1	1	2	1	1	1	2	1	1	1	2	1	1	1	2	1	1	1
2	1	1	1	2	1	1	1	2	1	1	1	2	1	1	1	2	1	1	1	2	2	2	2	2	1	1	1
2	1	1	1	2	1	1	1	2	1	1	1	2	1	1	1	2	1	1	1	2	1	1	1	2	1	1	1
2	1	1	1	2	1	1	1	2	1	1	1	2	1	1	1	2	1	1	1	2	1	1	1	2	2	2	2